SHEAR STRENGTH OF STEEL FIBER REINFORCED CONCRETE BEAMS

By

Mohammad Mousa Al-Khawaja

Supervisor

Dr.Yasser Hunaiti, Prof.

Co-Supervisor

Dr. Mohammad Al-Rjoub

Submitted in Partial Fulfillment of the Requirements for

Masters Degree of Science in Civil Engineering / Structures

University of Jordan

Faculty of Graduate Studies

January 2004

This thesis (SHEAR STRENGTH OF STEEL FIBER REINFORCED CONCRETE BEAMS) was defended successfully on 7th January 2004

Chairman of the Committee

Dr. Yasser Hunaiti
Professor of Civil Engineering _____
Jordan University

Member

Dr. Mohammad Al-Rjoub
Assistant Professor of Civil Engineering _____
AL Balqa University

Member

Dr. Hassan Saffarini
Professor of Civil Engineering _____
Jordan University

Member

Dr. Anis Shatnawi
Assistant Professor of Civil Engineering _____
Jordan University

Member

Dr. Yahia Abdel-Jawad
Associate Professor of Civil Engineering _____
Jordan University of Science and Technology

Dedication

To my family, my wife Amal, my sisters, my brothers, my father,to the soul of my mother , and to all who stood beside me.

Acknowledgments

The researcher wishes to express his deep appreciation and thanks to the supervisors Prof. Dr. Yasser Hunaiti and Dr. Mohammad Al-Rjoub for their expert guidance, assistance, valuable suggestions and continuous supervision during the whole course of this study.

The researcher would like to thank all the staff members of the civil engineering department especially members of the examining committee for their suggestions.

Finally, the researcher whishes to thank members of his family for their endless support.

Table of Content

Introduction

Previous Works

Behavior of Steel Fiber Reinforced Concrete

Derivation of The Governing Equations

List of Tables

List of Figures

ABSTRACT

SHEAR STRENGTH OF STEEL FIBER REINFORCED CONCRETE BEAMS

By

Mohammad Mousa Al-Khawaja

Supervised by

Prof. Dr. Yasser Hunaiti

Dr. Mohammad Al-Rjoub

Steel fibers (in concrete) have been used for many years to compensate the weakness in tension or diagonal tension (shear) of plain concrete members. Several researches were conducted to replace the conventional shear reinforcement (total or partially) by discrete steel fibers .

In this research a theoritical analysis has been conducted to study the shear strength of SFRC beams. Formulas are derived, in this work,using the Shear Failure Mechanism for slender beams and then extended to cover the deep beams

Since the failure mechanism include a splitting failure,a new formula is proposed to predict the tensile splitting strength of SFRC. The formula accounts for the concrete compressive strength , volumetric fiber content and the fiber aspect ratio.Also the size effects of the beams was introuduced to the derived equations.

A visual basic program is done , using the modified compression field theory to study the shear strength after accounting for the presence of the steel fibers .

In order to check the applicability of the proposed Equations, one hundred beams were analysed using the proposed equations.The predicted strengths are compared with the experimental values. Good agreement with the corresponding experimental values are noticed ,the comparisons of the shear predictions of this study are found comparable with those found in litrature.

Introduction

1. General

Fiber reinforcing has been used for many years. Many fibrous materials have been used as metallic (steel fibers) or non-metallic (carbon fibers, fiberglass, polymeric fibers). The beneficial effects of fiber reinforcement are to improve the mechanical properties such as toughness and strength and to cut the production costs by reducing or eliminating some forms of conventional reinforcement.

Fiber reinforced concrete is a whole class of materials rather than a single new type. Different combinations of fiber types, fiber contents and matrix compositions mixed using various production methods yield a vast range of material behavior. The mechanical behavior of the concrete may, due to change in fiber content alone, vary between being almost as brittle as plain concrete to being close to elastic-plastic or even deformation-hardening materials. Due to this feature of fiber reinforced concrete, the flexibility in changing the mechanical behavior for different uses, the material design is closely related with the structural design and vice versa.

The steel fibers as shown in Fig. 1 are either round or rectangular cross- section with deformed ends or deformed surfaces. The fiber length ranges from 6 mm to 75 mm and the aspect ratio of the fiber (length to thickness) varies from 30 to about 150. The volume fraction of fibers

ranges from 0 % to 3% with practically recommended limits not exceeding 1.5%.

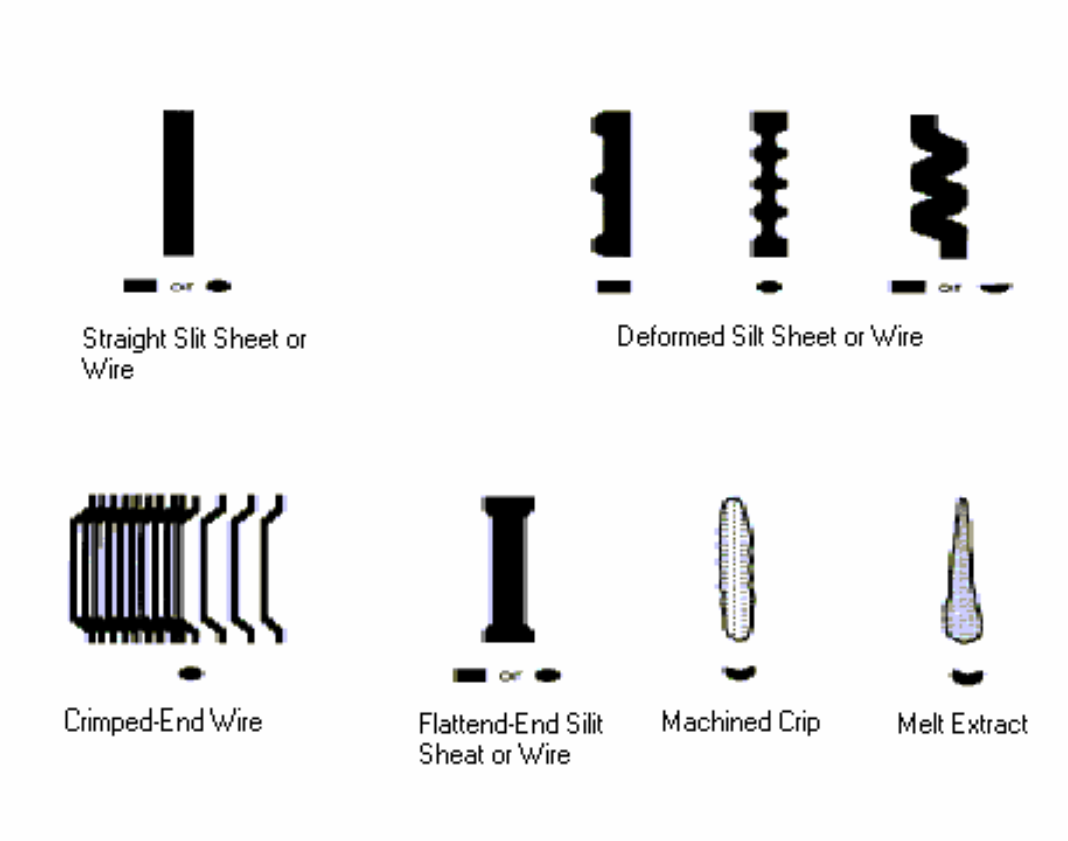

Figure 1: Types of steel fibers

The steel fiber reinforced concrete (SFRC) has been used in many applications in airports and highway paving and other plain structures where fibers act as crack distribution reinforcement. The random distribution of fibers arrests the micro cracks of SFRC, which controls the propagation and widening of the dowel cracks.

Several successful attempts were made to replace (partially or

totally) the conventional steel reinforcement especially for HSC beams. Furthermore the steel fibers are used in shotcrete applications that can be used in tunnels or repair of structures.

2. Shear Strength in SFRC

The use of fibers to improve the shear behavior of concrete is promising. Tests performed to study the shear behavior of SFRC can be categorized into two general groups: direct shear tests (Swamy 1987, Taan and Mansur 1990 and Amir et al. 2002), and tests on beams and corbels (Batson et al. 1972, Sharma 1986 and Kwak et al. 2002). The direct shear tests are performed to understand the basic transfer behavior of concrete, while the tests on beams are necessary to understand the behavior of structural members reinforced by fibers.

Tests showed that the addition of fibers generally improves the shear strength and ductility of concrete. Numerous research works like [Mansur et al 1986] reported that the shear reinforcement (stirrups) can be partially or totally replaced by the use of steel fibers. Most of the work has been limited to concrete of normal strength. The lack is even greater for research on shear strength of SFRC beams involving high strength concrete.

It is reported that the increase in shear strength can vary drastically depending on the geometry and properties of both the fibers and the

concrete matrix.

In general, fibers proved to be more efficient in high strength concrete than in normal strength concrete, by increasing both the ultimate load and overall ductility.

Despite the availability of some empirical relationships or experimental research that describe the shear strength of SFRC elements, more researches (analytical and experimental) are needed to develop a better understanding of shear behavior of fiber reinforced concrete elements.

3. Objectives and Scopes

This work is devoted to investigate the behavior of both normal and high strength SFRC beams subjected to shear. The current work will use the shear failure mechanism in the formulation of the shear strength of SFRC beams. The Major objectives of this work can be summarized as follows:

1. To formulate the shear strength of SFRC slender beams by studying the beam failure mechanism, accounting for the size effect.
2. To study the shear strength of the SFRC deep beams.
3. To study the shear strength of SFRC by extending the modified compression field theory (MCFT), that is used to study the

conventional RC, to account for the presence of steel fibers.

4. Layout of Thesis

The thesis consists of six chapters:

- A general introduction describing the effect of adding steel fibers on the mechanical properties (especially for the shear strength) of SFRC beams and the study objectives are presented in this chapter.
- Chapter two reviews the works found in literature that studied the shear strength of SFRC elements.
- The mechanical properties of SFRC material are presented in chapter three.
- The formulation of the governing equations is shown in chapter four.
- The proposed equations are verified in chapter five.
- Finally the conclusions and recommendations are summarized in chapter six.

Previous Works

Previous Works

1. General

The presence of steel fiber in concrete or mortar shows several potential advantages when used to supplement or replace the vertical stirrups or bent bars. This is caused by the random distribution of the steel fiber through the volume of concrete or the matrix, at which closer spacing than can be obtained with reinforcing bars. Also the shear friction strength, first crack tensile strength and the ultimate tensile strength are increased due to the presence of steel fibers.

2. Previous Works

In 1972 Batson et al. carried out a series of tests to determine the effectiveness of steel fibers as web reinforcement in small beams (100 x 150 x 2000 mm) with conventional flexural steel. The parameters they studied were the span to depth ratio (*a/d*), the fiber size, type, and fiber volume fraction content.

The study findings were, for shear-span-to depth ratio (*a/d*) of 4.8 the non-fiber beams failed in shear and developed a shear stress failure of 1.91 MPa, where for fiber fraction of 0.88%, the average shearing stress at failure was 2.14 MPa with a flexure-shear failure; for 1.76% fiber fraction

2.28 MPa with a moment failure, and for 2.66% volume 2.43 MPa, also with moment failure.

It was found that as the shear-span ratio decreased and fiber volume increased, higher shear stresses were developed at failure and a modification of failure mode occured.

In 1975 Paul and Sinnsmon studied the effect of the presence of straight steel fibers on the shear capacity of concrete in a series of seven tests similar to the work of Batson et al. [1972]. Their results agreed with those of Batson et al.

Sharma [1986] tested a set of seven beams with steel fiber reinforcement, of which, four beams contained stirrups. Based on his work and the works of Batson et al. [1972] and Williamson and Knab [1975], Sharma proposed the following equation for predicting the average shear stress, V_{cf} of steel fibers.

$$V_{cf} = \frac{2}{3} f_t' \left(\frac{d}{a}\right)^{1/4} \qquad (2.1)$$

Where:

d/a : The effective depth-to-shear-span ratio .

f_t' : The tensile strength of concrete obtained from results of indirect tension tests on 150 x 300 mm cylinders, (may be given as $0.79\sqrt{f_c'}$).

The simplicity of Eq. 2.1 makes it attractive, but this equation does

not explicitly account for other factors that are known to significantly influence the shear strength, as the fiber content, the shape of the fibers, aspect ratio (l_f/d_f) and the flexural reinforcement ratio.

Sharma found that the steel fibers are effective in increasing the shear strength of concrete, and steel fiber reinforced concrete beams have a high post-cracking strength, which is a desirable characteristic in design. Also SFRC beams have more ductility and significant toughness than that for conventional reinforced concrete beams. And the presence of fibers in concrete restricts the propagation of cracks and allows more uniform cracking.

Mansur et al. [1985] studied the shear strength of SFRC beams have no stirrups. The beams were made of normal strength and contain hooked ends steel fibers.

The conclusions showed that the beams have no fibers failed in shear for all *a/d* ratios. The inclusion of short fibers in the concrete matrix tends to change the failure mode from shear to flexure for higher values of *a/d.*

For a particular volume fraction of fibers it was noticed that, the mode of failure changes from shear to shear compression and then to diagonal tension and flexure when *a/d* ratio is increased.

Further more, the higher values of the longitudinal reinforcement ratio, ρ induces shear failure because longitudinal bar reinforcement contributes more to the bending than to the shear resistance of a beam. Similarly the presence of fibers, in higher concrete strength increases the shear resistance more than the corresponding increases in the bending moment capacity.

Mansur et al. [1986] developed the following equation for predicting the shear strength of fibrous concrete

$$V = V_c + V_{sy} \tag{2.2}$$

Where:

V_c: shear resistance of concrete.

V_{sy}: shear resistance due to web reinforcement.

They considered that shear strength of fibrous concrete beams consists of two parts; the first term is adopted from ACI Building Code [2002] Eq. (11.5), where the concrete strength of reinforced concrete V_c can be calculated as follows:

$$V_c = \left(0.16\sqrt{f_c'} + 17.2\frac{\rho V d}{M}\right)bd < \left(0.29\sqrt{f_c'}\right)bd \tag{2.3}$$

Where:

$f_c^{'}$: Standard compressive strength of concrete (MPa).

ρ: Percentage of longitudinal reinforcement steel

An additional shear strength σ_{tu}, caused by the presence of steel fibers, is added to that obtained from Eq.2.2 of the conventional RC.

Mansur substituted the contribution of the conventional shear reinforcement, V_{sy} by the contribution of steel fibers, ($\sigma_{tu} bd$). So Eq. 2.2 is rewritten in the following form

$$V_n = V_c + \sigma_{tu} bd \qquad (2.4)$$

Where σ_{tu} is the stress after crack formation calculated as the difference between splitting strength of normal concrete and fibrous specimens.

The term σ_{tu} depends on many factors such as the fiber content, aspect ratio, surface characteristics of the fibers and the maximum aggregate size.

In 1987 Narayanan and Darwish studied the behavior of steel fiber reinforced concrete beams subjected to predominant shear, by testing experimentally 49 simply supported rectangular beams loaded by two symmetrically concentrated loads.

For comparison purpose, they tested 10 beams with conventional stirrups, while the remaining beams contained fibers of variable volume fraction V_f, and aspect ratio l_f/d_f, variable concrete strength f'_c and different longitudinal steel ratios $\rho\%$.

Their findings showed an improvement of the ultimate shear strength of beams containing steel fibers up to V_f=1% compared with those contained conventional stirrups, and a significant increase of the first crack shear strength due to the crack arresting mechanism of the fibers. Also the study reported that any increase in the fiber volume more than 1% did not significantly improve the shear strength.

Based on these tests and data obtained by other researchers they proposed an empirical equation to evaluate the ultimate shear strength of SFRC beams.

$$v_u = e\left[0.24 f'_{spfc} + 80\rho\frac{d}{a}\right] + v_b \qquad (2.5)$$

Where:

a/d = Shear span to depth ratio.

f'_{spfc} = Split cylinder strength of (SFRC). $f'_{spfc} = \frac{f_{cuf}}{\left(20-\sqrt{F}\right)} + 0.7 + \sqrt{F}$

F = Fiber factor = $(l_f/d_f)\, V_f\, D_f$

l_f / d_f = Fiber length to diameter

D_f =Bond factor equals 0.50 for round fibers, 0.75 for crimped fibers, and 1.00 for indented fibers.

V_f = Volume percentage of steel fibers.

ρ = Percentage of longitudinal tensile reinforcement.

f_{cuf} = The cubic strength of fiber reinforced concrete, in MPa.

e=None dimensional factor equals 1.0 when $a/d > 2.5$,and $2.5\ d/a$ when $a/d < 2.5$.

$V_b = 0.41\ \tau F$

τ = Average fiber matrix interfacial stress taken as 4.15 MPa.

According to Narayanan and Darwish, the first term in brackets in Eq. 2.5 accounts for the fiber contribution in terms of the split cylinder strength, the second term accounts for the dowel action. The third term accounts for the contribution of fibers across the inclined crack.

Ashour et al. [1992] studied the behavior of high-strength concrete beams containing steel fiber instead of shear reinforcement by testing under the action of flexure and shear.

The authors observed that the behavior of concrete beam subjected to bending and shear is affected by the shear-span to depth ratio (*a/d*). The addition of fibers enhances the mechanical and structural properties of

normal as well as high-strength concrete beams. Also the tested beams exhibited failure modes similar to conventional beams (without fibers), but the presence of high percentage of steel fibers transformed the failure mode into a more ductile. The beams of moderate length beams (where 3 <*a/d* < 6) with no fibers failed soon after the formation of the first diagonal cracks. The steel fibers became more effective after the formation of shear cracks that continued to resist the principal tensile stresses until the complete pullout of all fibers occurred on one critical crack.

Test results showed also that increasing the fiber content increases the shear strength. The rate of increase was higher as *a/d* became smaller. Ashour et al. proposed the following equations, as a modification of the known Zsutty's equation as

For $a/d > 2.5$

$$v_u = \left(2.11\sqrt[3]{f_c'} + 7F\right)\left(\frac{\rho d}{a}\right)^{0.333} \qquad (2.6)$$

For $a/d < 2.5$

$$v_u = \left(2.11\sqrt[3]{f_c'} + 7F\right)\left(\frac{\rho d}{a}\right)^{0.333}\left(\frac{2.5}{a/d}\right) + v_b\left(2.5 - a/d\right) \qquad (2.7)$$

Where the parameters F, f'_c, a, d and ρ are the same parameters mentioned earlier.

Kwak et al. [2002] tested experimentally twelve simply supported beams containing three hooked steel fiber-volume fraction V_f (0, 0.5 and 0.75 %), and three span-depth ratio *a/d* (2,3 and 4), and two compressive strengths (31 and 65 MPa), Kwak et al. [2002] reported that the nominal stress at first shear cracking and the ultimate shear strength increased with increasing fiber content.

They reported also that the increase of steel fiber would change the nature of failure mode; compared with that of conventional RC beams (without steel fibers).

Kwak et al. [2002] proposed the following empirical equation that predicts the shear strength of SFRC beams as follows :

$$v_u = 2.1 e f_{spfc}^{0.7} \left(\rho \frac{d}{a} \right)^{0.22} + 0.8 v_b^{0.97} \qquad (2.8)$$

Where: *a, d, F,* d_f, l_f, D_f, V_f, ρ, f'_{spfc}, f_{cuf}, and v_b are the same as the parameters Mentioned in Narayanan and Darwish [1978].

e=None dimensional factor equals 1.0 when *a/d* > 3.5, and 3.5 *d/a* when *a/d* < 3.5.

Noghabi [2000] conducted a study on high strength reinforced

concrete beams loaded by shear and bending moments. Various types of fibers were added to the concrete matrix up to 1% per volume of concrete. Four sizes of beam depths and lengths were used. (d= 195 to 410 mm and beam span = 1.2 to 5 m).

It is found that the fiber cocktail (mixing fibers with different aspect ratios) improves more than using a single type of fiber, and the chosen steel fibers are competitive with the conventional stirrups.

Amir et al. [2002] studied the shear strength of steel fiber reinforced concrete using the direct shear method. The tested specimens contained fiber with volume fraction ranged from 0% to 2%. The study showed that significant improvements are obtained as the volume of fiber increased. The study suggested that the ultimate shear strength τ_{max} to be given by the formula

$$\tau_{\max} = \tau_o + k V_f^{\,n} \qquad (2.9)$$

Where τ_o: is the shear strength of the plain concrete. k equals 4.29 for flattened end fibers and 2.9 for crimped geometry fibers.

V_f: is the volume fraction of fiber.

n: equals 1 for flattened end fibers and 0.5 for crimped geometry.

3. Shear Failure Mechanism Studies

Despite the fact that all experimental studies of the works mentioned in the previous sections describe the failure mechanisms and modes, the proposed formulation are founded on empirical or semi-empirical equations that expresses the shear strengths on terms of the direct or indirect tensile strengths.

On the other hand several studies attempted to study the behavior of shear elements and predict their shear strength by studying the crack mechanism. Among those, the Modified Compression Field Theory (MCFT) [Vecchio and Collins 1986] was developed to predict the load deformation response of RC members loaded by shear or shear combined with torsion.

Also, Zararis [1988,1995] studied the failure mechanism to predict the shear strength of RC plates. The failures due to yielding of steel reinforcement as well as the failure caused by concrete crushing were checked. The predicted ultimate loads showed very good agreement with the experimental values. He extended the failure mechanism to predict the shear strengths of beams with and without shear reinforcement [Zararis 2001, Zararis 2003]

A simple expression was derived to determine the shear strengths of slender beams have no shear reinforcement [Zararis 2001] and beams

containing stirrups [Zararis 2003]. The proposed formulas were verified through the comparisons with experimental data from literature.

Since the failure mechanisms of RC beams are approximately similar to that of SFRC, the failure mechanism approach used in RC beams is to be extended to cover the SFRC beams after introducing the effect of presence of steel fibers in concrete matrix, which is to be covered in this thesis.

Behavior of Steel Fiber Reinforced Concrete

1. General

Steel fiber reinforced concrete (SFRC) is made of hydraulic cement containing coarse aggregate and discontinuous discrete steel fibers (ACI 544R 1994). The concrete used in the mixture is of a usual type, also the proportions should be varied to obtain good workability and take full advantage of the fibers. This may require limiting the aggregate size, optimizing gradation, increasing the cement content and adding admixtures to improve workability.

The fibers may take many shapes. Their cross section includes circular, rectangular, half round and irregular or varying cross section. They may be straight or bent, and come in various lengths. A conventional numerical parameter called the aspect ratio is used to describe the fiber length to diameter ratio; this may vary from 30 to about 150. Fibers have been produced from steel, plastic, glass and natural materials of various shapes and types.

The SFRC mixtures use from 0.25 to 1.5 volume percent fibers. Two major reasons are intended by adding fibers to the conventional concrete: the first is to produce a stiffer composite material and the second is to hold the matrix together after it cracks. The strength of the cracked composite may therefore be significantly increased and the toughness as well as the ductility of the new material will be improved.

SFRC may be best thought of as a concrete with increased strain capacity, impact resistance, energy absorption, and tensile strength. The increase in these properties may vary from substantial to insignificant depending on the quality and types of added fibers. Full-scale tests have shown that steel fibers are effective in supplementing or replacing the stirrups in beams (Craig 1993 and Sharma 1986).

The strengthening mechanism of the fibers involves transfer of stress from the matrix to the fibers by interfacial shear or by interlock between the fiber and the matrix. Thus the stress is shared by the fiber and matrix in tension until the matrix cracks and the total stress is progressively transformed to the fiber.

An understanding of the mechanical properties of SFRC and their variation with fiber type and content is an important aspect of a successful analysis and design. These properties are discussed in the following sections.

2. Compressive Strength of SFRC

The compressive properties of steel fiber reinforced concrete (SFRC) are relatively less affected by the presence of fibers as compared to the properties under tension and bending.

The influence of fibers in improving the compressive strength of the matrix depends on whether mortar or concrete is used and on the magnitude of compressive strength. Studies prior to 1988 showed that with the addition of fibers there is an almost negligible increase in strength for mortar mixes; however for concrete mixes, strength increases by as much as 23%. Furthermore, Otter and Naaman [1988] showed that use of steel fibers in lower strength concretes increases their compressive strength significantly compared to plain unreinforced matrices and is directly related to volume fraction of steel fiber used. This increase is more for hooked fibers in comparison with straight steel fibers, glass or polypropylene

fibers. The typical influence of fibers on the stress- strain curve of concrete composites is shown in Fig 2.

Ezeldin and Balaguru [1992] conducted tests to obtain the complete stress-strain curves of steel fiber-reinforced concrete with compressive strengths ranging from 35 MPa to 84 MPa. The matrix consisted of concrete rather than mortar. Three volume fiber fractions and three aspect ratios were investigated. It was reported that the addition of hooked-end steel fibers to concrete, with or without silica fume, marginally increased the compressive strength and the strain corresponding to peak stress.

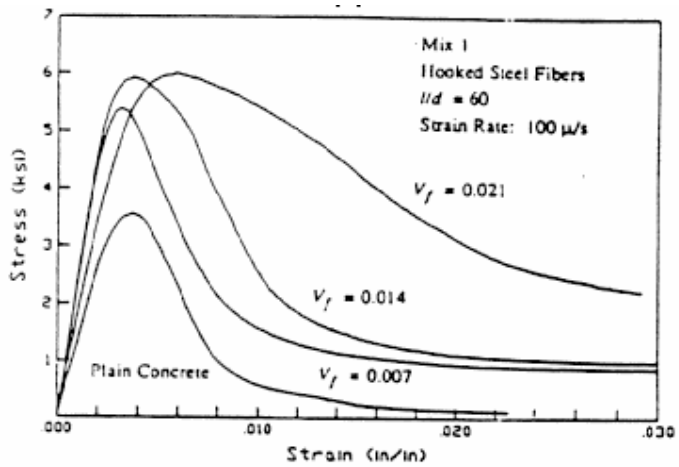

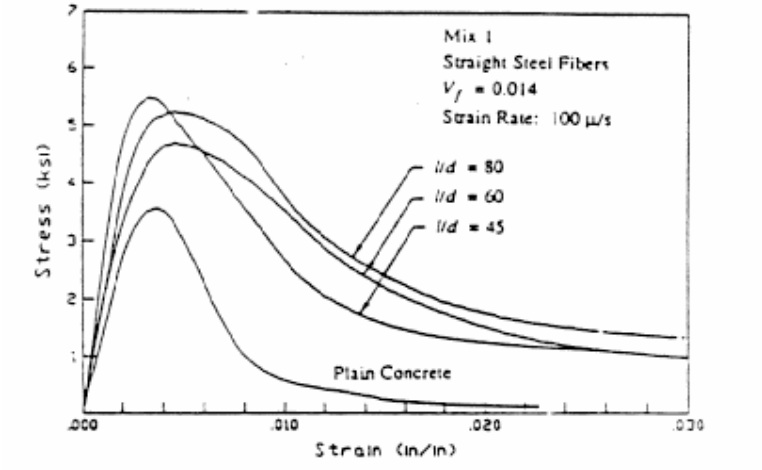

Figure 2: Stress-strain response of SFRC under compression (a) hooked steel fibers; (b) straight steel fibers [Otter and Naaman 1988]

The increase in fiber content causes an increase in the compressive strength of SFRC ranging from 5% to 25% [Ezeldin and Lowe 1991].

3. Tensile Strength of SFRC

Tension failure of cement-based matrices is rather brittle and the associated strains are relatively small in magnitude. The addition of fibers to such matrices, whether in continuous or discontinuous form, leads to a substantial improvement in the tensile strength of the SFRC in comparison with the properties of the unreinforced matrix. The enhancement of the properties is particularly noticeable.

The stress–strain or load–elongation response of fiber composites in tension depends mainly on the volume fraction of fibers. Typical stress–

strain or load–elongation curve for conventional SFRC Composites are shown in Fig. 3. In general, the response can be divided into two or three stages, depending on whether the composite is SFRC (fiber volume less than about 3%). These stages are summarized as follows:

Before cracking, the SFRC can be described as an elastic material with a stress–strain response very similar to that of the un-reinforced matrix.

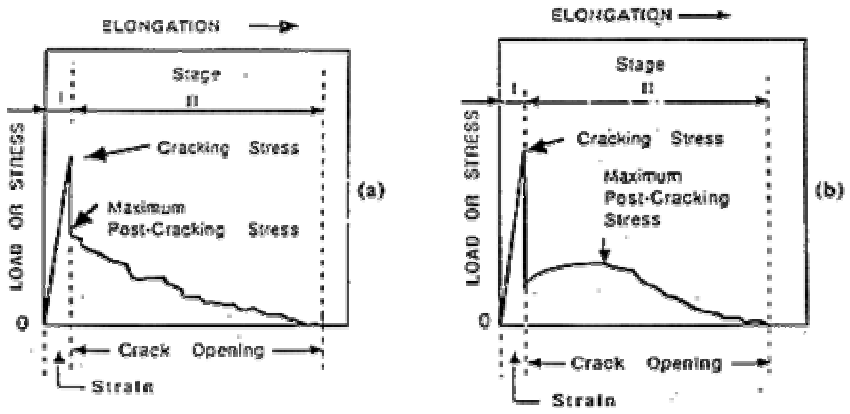

Figure 3: Typical load-elongation response in tension of fiber reinforced concrete; (a) using premixed steel fibers, and (b) using premixed polypropylene fibers [Naaman 1985].

After cracking and in bridging the cracked surface, the fibers tend to pull out under load resulting in a sudden change in the load–elongation or stress–strain curve.

Beyond the peak point, a third stage of behavior exists characterized by failure and/or pullout of the fibers about a single critical

crack. The corresponding descending branch of the load–elongation curve can be steep or of moderate slope depending on the fiber reinforcing parameters and whether a brittle or ductile failure occurs.

The multiple cracking stage described above occurs only if the maximum post cracking stress is larger than the cracking stress; otherwise, in the case of conventional SFRC, with a relatively small volume fraction of fibers, the second portion of the curve vanishes and is replaced by a sudden drop in the load–elongation curve joining the cracking load to the post cracking load. Hence the load–elongation response is reduced to two main parts (stages I and II) as illustrated in Fig 3.

4. Flexural Strength of SFRC

The presence of steel fibers affects the flexural strength of concrete much greater than the direct tension or compression. The ultimate strength in flexure could vary considerably depending upon the volume fraction of fibers, length and bond characteristics of the fibers and the ultimate strength of the fibers. Depending upon the contribution of these influencing factors, the ultimate strength of SFRC could be either smaller or larger than its first cracking strength.

Generally, there are three stages of the load-deflection response of SFRC specimens tested in flexure and schematically they are shown in Fig. 4.

The first stage is linear up to point A. The strengthening mechanism in this portion of the behavior involves a transfer of stress from the matrix to the fibers by interfacial shear. The imposed stress is shared between the matrix and fibers until the initiation of the first cracks where the matrix starts to crack.

Figure 4: Schematic load-deflection diagrams of SFRC.

Then a transition nonlinear portion between point A and the maximum load capacity at point B is encountered. In this stage, which occurs after cracking, the stress in the matrix is progressively transferred to the fibers. As the load increases, the fibers tend to gradually pull out from

the matrix leading to a nonlinear load–deflection response until the ultimate flexural load capacity (peak strength) at point B is reached.

The stage represents the post peak descending portion, which starts from the peak strength and continues until the complete failure of the composite. This part refers to the degree at which loss in strength is encountered. As the deformation increases it reflects also an important indication of the ability of the fiber composite to absorb large amounts of energy before failure occurs.

The nonlinear portion between A and B exists only if a sufficient volume fraction of fibers is present. For low volume fraction of fibers ($V_f <$ 0.5%), the ultimate flexural strength coincides with the first cracking strength and the load–deflection curve descends immediately after the cracking load. Typical load–deflection curves of SFRC beams observed experimentally for different types of fibers are shown in Figure 3.4

Ezeldin and Lowe [1991] studied the flexural strength properties of rapid-set materials reinforced with steel fibers. Four fiber types made of low-carbon steel were incorporated in their study. Two were hooked and one was crimped at the ends, and the fourth was crimped throughout the length. Through out their study an increase in the flexural strength was observed. The fiber efficiency in enhancing the flexural strength is controlled by the fiber surface deformation, aspect ratio, and fiber content.

5. Modulus of Elasticity

The modulus of elasticity of a material, whether in tension, compression, or shear, is a fundamental property that is needed for modeling mechanical behavior in various structural applications.

Numerous studies have addressed the modulus of elasticity of composite materials. They lead to several models that range from the very simple to the very sophisticated. Among the simplest models for composites made out of two different materials, the upper- and lower-bound solutions or a combination of them (described below) only depend on the volume fraction and the modulus of each material. More advanced models developed for fiber reinforced composites include, in addition to the properties of the interface between the two materials, the fiber distribution and orientation of fibers, the aspect ratio, and whether the fibers are discontinuous or not.

The most common and the simplest models to predict the modulus of elasticity of SFRC as a composite made out of two materials are the upper-and the lower-bound solutions or an arithmetic combination of both.

The upper-bound solution assumes that the fibers are continuous and oriented in the direction of loading along which the modulus of elasticity is studied. It leads to the following equation:

$$E_{cl} = E_f V_f + E_m \left(1 - V_f\right) \tag{3.1}$$

in which the subscripts c, L, f, and m stand respectively for composite, longitudinal, fiber, and matrix.

The lower bound solution assumes that the fibers are lumped with their axis normal to the direction along which the modulus is measured. It leads to the following equation:

$$E_{cT} = E_f E_m / \left[\left(1 - V_f\right) + V_f E_m\right] \tag{3.2}$$

in which the subscript T stands for transverse.

For a composite with randomly oriented fibers, Halpin and Tsai [1969] suggested an equation based on a combination of Eqs. (3.1) and (3.2). Although their predictions of longitudinal and transverse moduli were different from the above upper- and lower-bound solutions, their equation can be used as a first approximation with the above equations. It is given by:

$$E_c = \left(\frac{3}{8}\right) E_{cL} + \left(\frac{5}{8}\right) E_{cT} \qquad (3.3)$$

Experimental studies [Fanella and Naaman 1985; Shah et al. 1978] have shown that the addition of fibers have only a slight effect on the ascending branch (modulus of elasticity) of the stress–strain curve of the composite. Patton and Whittaker 1983 have also observed that the effect of adding fibers up to 4% by volume is small and linear for composites tested in flexure.

6. Strain Capacity

The ability to withstand relatively large strains before failure, the superior resistance to crack propagation and the ability to withstand large deformations and ductility are characteristics that distinguish fiber-reinforced concrete from plain concrete. These characteristics are generally described by "toughness" which is the main reason for using fiber-reinforced concrete in most of its applications.

Unlike plain concrete specimens, the presence of fibers imparts considerable energy to stretch and debond the fibers before complete fracture of the material occurs. Toughness is a measure of the ability of the

material to absorb large amounts of post-elastic strains or deformations prior to failure. Typical load–deflection curves of SFRC specimens in comparison with plain concrete specimens are shown in Fig. 5.

ASTM-C 1018 provides Method A for evaluating the toughness of fiber reinforced composites through the use of a toughness index. The toughness index is calculated as the area under the load–deflection curve up to the prescribed service deflection divided by the area under the load–deflection curve up to the first cracking deflection. Three indices are described in ASTM-C 1018: I_5, I_{10} and I_{20} corresponding respectively to deflections of 3, 5.5 and 10.5 times the deflection at first cracking.

These indices (computed as shown in Fig. 5) provide indications of the shape of the load–deflection response (post cracking) and available ductility. It should be emphasized that the values of I_5, I_{10} and I_{20} are unity for elastic, perfectly brittle material behavior and is equal to 5, 10 and 20 respectively for elastic, perfectly plastic material behavior.

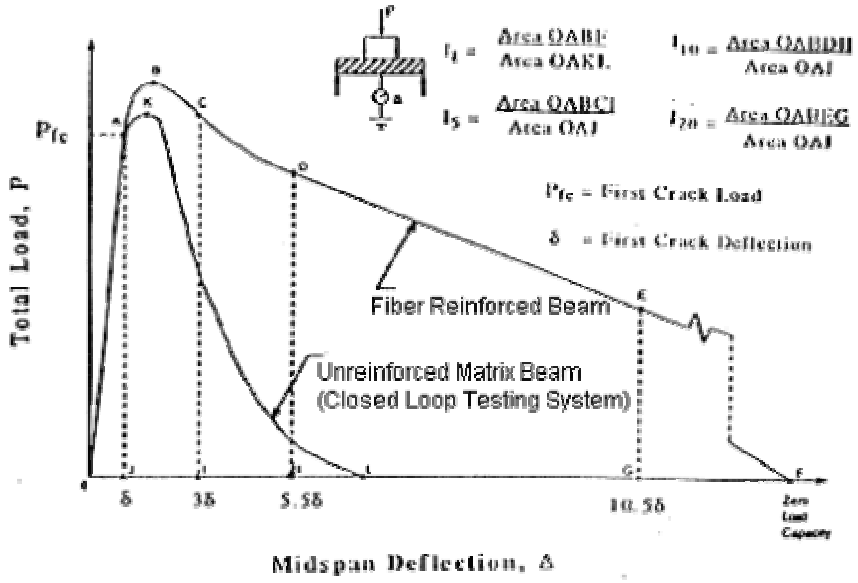

Figure 5: Toughness indexes from flexure load-deflection diagram.

The same variables that affect the ultimate flexural strength of SFRC beams also influence the flexural toughness; namely, the type of fiber, the volume fraction of fiber, the aspect ratio, the fiber's surface deformation, bond characteristics and orientation.

Balgaru et al. [1992] studied the flexural behavior of steel fiber reinforced concrete. The focus was on the toughness behavior. It was noted that addition of silica fume improves the strength and slightly reduces ductility. The study concluded that the increase in fiber content results in consistent increase in ductility and energy-absorption capacity. The post peak load–deflection responses are flatter and the toughness indices are higher.

In addition to the Toughness Indexes 5 and 10 computed using the ASTM procedure are not sensitive enough to show the variations that are present in the load–deflection responses. If deflections are measured accurately, values 50 and 100 can be computed for all fiber types and fiber contents greater than or equal to 30 kg/m^3. Also the Higher fiber contents result in much higher load-retaining capacity at large deflections. In almost all cases, there was a considerable difference in the 100 values between fiber contents. For a given fiber content, toughness indices are smaller for high-strength concretes compared to normal strength concretes. The differences are less significant at higher fiber volume fractions.

7. Poisson's Ratio

Little information exists on the Poisson's ratio of fiber-reinforced concrete. In most analytical studies, the Poisson's ratio is generally assumed to be the same as that for concrete. This may be a reasonable assumption provided that the composite remains in the elastic range of behavior. As soon as cracking develops, the confining effects of the fibers bridging the cracks will have a significant effect on the lateral deformation, consequently on the value of the measured Poisson's ratio.

Derivation of The Governing Equations

1. General

Despite the extensive studies the problem of how shear failure occur in RC as well as SFRC, remains unresolved. And the shear in the design codes [ACI-02, CEB-FIP] is based on empirical or semi-empirical considerations.

In this chapter, an attempt is made to derive equations that govern the failure mechanism of SFRC beams of no stirrups. The approach that was derived firstly by Zararis for conventional RC plates [1988, 1995] and for RC beams [2001, 2003] is applied in this research work for SFRC beams, since the failure mechanisms for RC and SFRC are almost alike.

In this study the influence of steel fiber on increasing the modulus of rupture, (that in turn affects the depth of the compression block), as well as the splitting strength of steel fibers and the size effect are found and introduced to the governing equations.

Also, the formulation of the modified compression field theory (MCFT) [Vecchio and Collins, 1986] after accounting for the influence of adding steel fibers is presented and applied, especially for deep beams.

2. Shear Strength Based on Failure Mechanism (Slender Beams):

2.1 Critical and Diagonal Crack Characteristics

The critical failure cracks in slender beams have no shear reinforcement under two-point loading; involve two branches as shown Fig. 6. Normally, these two branches are formed at different time instants and are due to different causes. The first branch is an inclined shear crack, which develops after the onset of nearby flexural cracking.

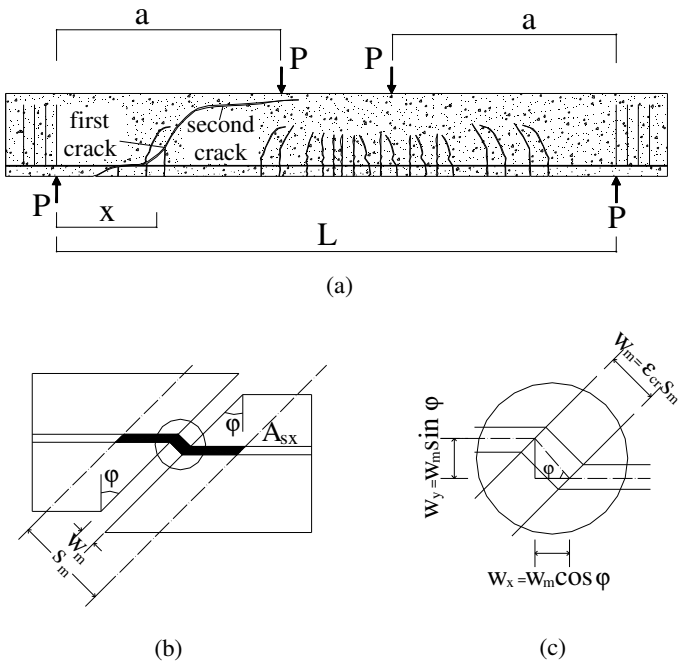

Figure 6: (*a) Crack pattern of simply supported beam under two-point loading (b) Simplified equivalent deformation of steel(c) Details.*

The failure in slender beams is caused by the formation of the second branch of the critical crack, which initiates from the tip of the first branch and propagates toward the load point crossing the compression

zone. This mode of failure is conventionally called diagonal tension failure, that occurs in slender beams [where shear span to depth ratio *(a/d)* > 2.5].

The analytical expressions derived in this chapter describe the characteristics of these two branches, as well as the shear failure mechanism.

2.2 Stresses and Forces on The first Branch of Shear Crack

Throughout the study of failure mechanism in RC plates, Zararis [1988,1995] showed that by the formation of the first crack, there will be a strain transverse to the crack due to the orthogonal crack opening mentioned earlier. The opening of the first branch shear crack is assumed to be perpendicular to its direction.

A simplified equivalent deformation of steel bars at the crack location is shown in Fig. 6 (c). If the initial crack direction forms an angle ϕ with the transverse axis (Y-axis), and the steel stresses (in this stage) obeys Hook's law, then $\sigma = \varepsilon E$ and $\tau = G\,\gamma$ where:

σ, τ: normal and shear stresses.

E, G: are Hooks and shear rigidity moduli of elasticity, in which *G* is given by $G = E/2(1+\nu)$, and ν is Poisson's ratio.

ε , γ: are the normal and shear strains.

The normal stress in x-direction and the shear of steel bars can be given by:

$$\sigma_{sx} = E_s \varepsilon_s \tag{4.1-a}$$

$$\tau_{sxy} = G_s \gamma_{xy} \tag{4.1-b}$$

Where:

$$\varepsilon_s = \frac{w_x}{s_m / \cos\varphi} \;,\; \gamma_{xy} = \frac{w_y}{s_m / \cos\varphi}$$

w_x, w_y, φ, s_m are shown in Fig. 6.

The compression zone exists above the tip of the first branch of the critical crack. This solid zone essentially acts as a buffer preventing any meaningful contribution of shear slip along the crack interface. So, at this stage no aggregate interlock and dowel forces develop. If the value of poisson's ratio is taken equal to 0.3 and the strains (ε_x and ε_y) are written in terms of the strain orthogonal to the crack direction ε_{cr}, then Eq. 4.1 can be rewritten in the form:

$$\sigma_{sx} = E_s \; \varepsilon_{cr} \cos^2\varphi \tag{4.2-a}$$

$$\tau_{sxy} = 0.4 E_s \varepsilon_{cr} \cos\varphi \sin\varphi \tag{4.2-b}$$

The substitution of $E_s \varepsilon_{cr}$ of Eq. 4.2-a into Eq. 4.2-b leads to the following relationship that expresses shear stresses in term of the longitudinal normal stresses of steel.

$$\tau_{sxy} = 0.4\, \sigma_{sx} \tan\varphi \qquad (4.3)$$

The multiplication of the stresses τ_{sxy} and σ_{sx} by the area of steel A_s, produces the shear and normal forces in the steel V_d and T, respectively, and the following equation is obtained.

$$V_d = 0.4\, T \tan\varphi \qquad (4.4)$$

This analysis implies that the shear force of steel bars at a crack location is caused by a pure shearing deformation of the bars and is not due to a kinking or a slip of crack faces.

Due to the assumption of orthogonal crack opening, the normal force T and shear force V_d, of steel bars are the only forces acting on the faces of the first branch of the critical diagonal crack. On the other hand, the normal and shear concrete forces in the compression zone, C and V_c, respectively, are also depicted.

2.3 Height of the First Branch of Shear Crack

From the strain distribution shown in Fig. 7-e one can obtain the following:

$$\frac{\varepsilon_c}{\varepsilon_s} = \frac{c}{d-c} \qquad (4.5)$$

Where c = is the depth of compression zone above the tip of the diagonal crack, d = is the effective depth to the longitudinal flexural reinforcement; and ε_c = is the concrete strain of extreme fiber in compression.

From the equilibrium of forces acting on the triangular concrete element below the tip of an inclined shear crack, shown in Fig. 7(b), it can be seen that concrete compressive stresses are also involved below the tip of the inclined crack on the vertical section of the beam. These stresses are transferred from the top fiber of the beam to the area below the tip of the diagonal crack. This explains the presence of compressive force ΔT in Fig. 7(b).

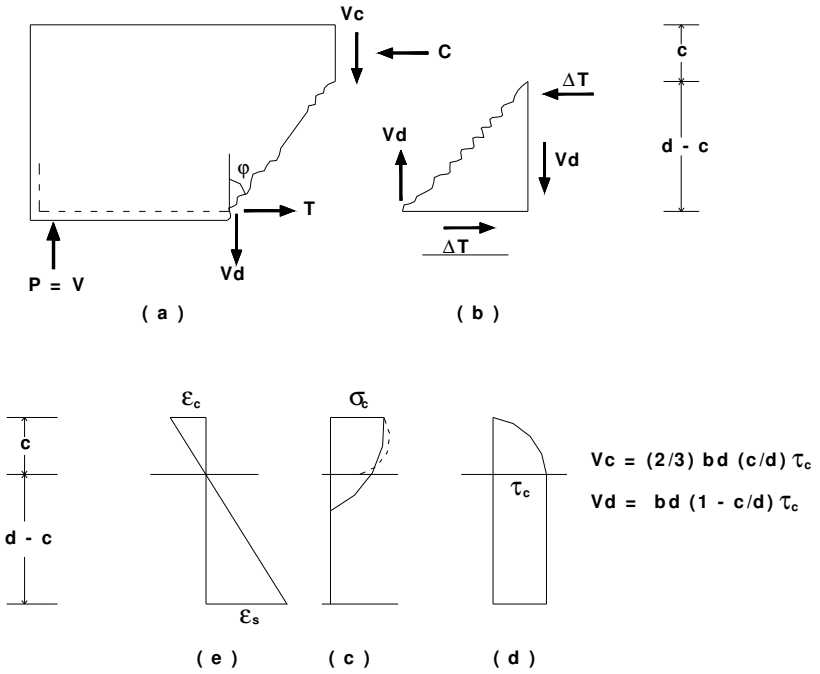

Figure 7:Forces and stresses at the inclined crack (a) Forces on the left hand side of the cracked beam (b) Forces on triangular concrete element (c) concrete compressive stresses along depth of beam (d) concrete shear stresses along beam depth (e) Strain distribution.

The concrete compressive stresses above the tip of the diagonal crack form a parabolic curve shown in Fig. 7(c).

The resultant of the concrete compressive stress of this block is equal to the normal steel force *T* at the diagonal crack. So, the variation of (*c/d*) with ε_c is very small, and it is reasonable to use a single value of *(c/d)* for all values of ε_c. For convenience this value is taken equal the peak strain. ε_{co}, (the strain that corresponds to the ultimate concrete strength). According to ACI-Code [2002] the value of ε_{co} is equal to 0.002, and the

corresponding resultant of concrete stresses in compression with width *b* is $C = (2/3)\, b\, c\, f'_c$.

Then, equating the normal steel force *T* with the force *C* and taking into account Eq.4.5 after substituting E_s = 2 X 10^5 MPa, yields the following equation:

$$\left(\frac{c}{d}\right)^2 + 600\frac{\rho}{f'_c}\frac{c}{d} - 600\frac{\rho}{f'_c} = 0 \qquad (4.6)$$

Where ρ = steel ratio, and f'_c = concrete compressive strength in MPa.

2.4 Angle at First Branch of Critical Crack

The resultant of the shear distribution shown in Fig.7 (d) equals the total external shear force *V*, so

$$V = V_c + V_d \qquad (4.7)$$

Where:

$$V_c = \frac{2}{3} bd \frac{c}{d} \tau_c \qquad (4.8\text{-a})$$

$$V_d = bd\left(1 - \frac{c}{d}\right)\tau_c \qquad (4.8\text{-b})$$

The substitution of τ_c from Eq.4.8 (a) into Eq.4.8 (b) and substituting V_c by V-V_d, yields the following equation that expresses the shear force in the steel

$$V_d = V\left(1-\frac{c}{d}\right)\Big/\left(1-\frac{1}{3}\frac{c}{d}\right) \qquad (4.9)$$

Fig. 8(a) shows the line of compressive action of the resultant of the concentrated load P and the normal concrete force C_f in the region of pure bending, which passes diagonally the shear span, a. If the tip of an inclined shear crack is on this diagonal line, the resultant of the concrete forces (P and C_f) shown in Fig. 8(b), will also be lying on the line of compressive action, this resultant causes a type of splitting of concrete along this line, featuring a crack that initiates from the tip of the inclined crack and propagates along this line of compressive action toward the area of the point of load, P. This can be analytically explained based on the theory of elasticity, as will be described in the following section.

The above consideration constitutes a necessary condition for the shear failure of the beam. This condition requires that the summation of the moments (about the tip of the inclined crack) of the forces acting on the beam portion shown in Fig. 8(b) be equal to zero.

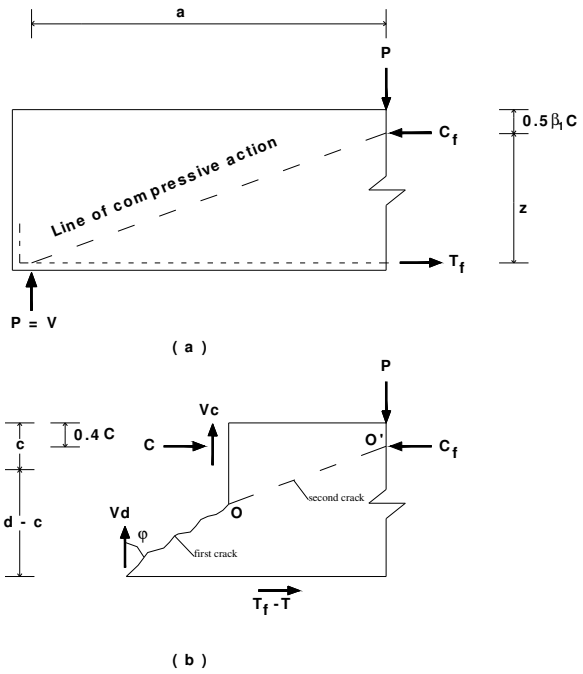

Figure 8: Diagonally compressed concrete areas: (a) line of diagonal compressive action: (b) Forces on portion of beam where splitting occurs.

The distance of the normal concrete force C_f from the compressed fiber in the region of pure bending according to ACI code (ACI 2002) is $0.5\beta_1 c$, where $\beta_1 c$ = depth of the equivalent rectangular stress block. The factor β_1= 0.65 to 0.85, depending on the value of concrete strength f'_c. Assuming a mean value β_1= 0.72 for all values of f'_c, the summation of forces acting on the portion of beam shown in Fig. 8(a) along x-axis, leads to a steel force T_f in the region of pure bending equals T_f equals P $(a/d)/(1-0.36c/d)$.

Also taking into account Eq 4.4 and equating the compressive force C by the tensile force T, the following equation is obtained

$$V_d = \frac{V\left(1-\frac{c}{d}\right)\tan\varphi}{\left[2.5-c/d+(1-c/d)\tan^2\varphi\right](1-0.36c/d)} \qquad (4.10)$$

A division by sides of Eq. (4.9) and Eq. (4.10), and assuming *1-0.36c/d ≅ 1- (1/3) c/d* yields

$$\tan^2\varphi - \frac{a/d}{1-c/d}\tan\varphi + \frac{2.5-c/d}{1-c/d} = 0 \qquad (4.11)$$

The angle φ of the first branch of the critical crack corresponds to the positive root of Eq. 4.11.

2.5 Distance of Critical Crack from Support

Since the tip of the first branch of the critical diagonal crack is on the line of the compressive action, the distance *x* that corresponds to the first critical diagonal crack from the support can be obtained by geometrical relations from the sketches shown in Fig.9

$$\frac{x}{d} = \left(1-\frac{c}{d}\right)\left(\frac{a/d}{1-0.36c/d} - \tan\varphi\right) \qquad (4.12)$$

2.6 Splitting Failure (second branch or critical crack)

The equilibrium of forces acting on the portion of beam shown in Fig.9 implies that only normal stress exist along this line of the second branch, which represents a group of forces acting in self-equilibrium. Such a stress distribution implies a failure due to splitting of concrete in this area.

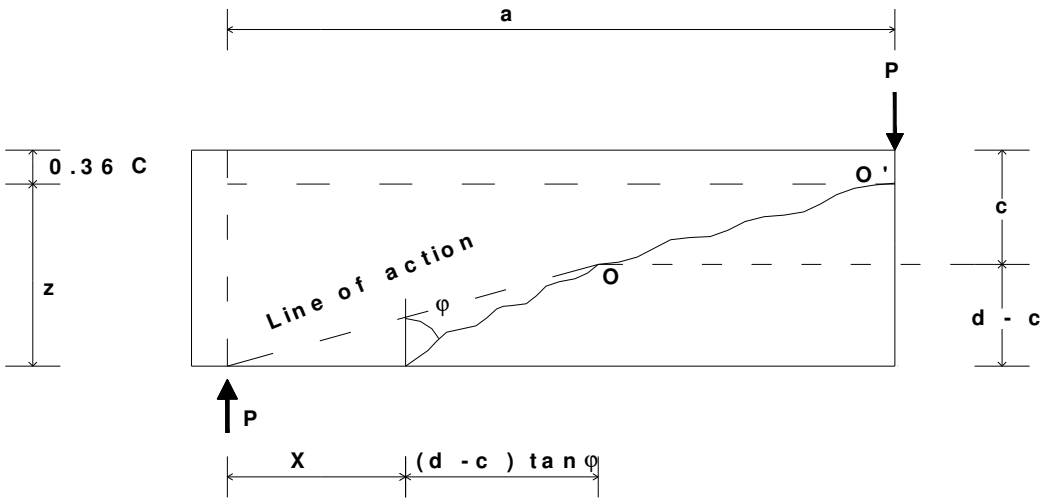

Figure 9: Geometrical representation of critical diagonal cracks.

A possible arrangement of the concrete forces acting in the region of the beam where the splitting of concrete occurs as shown in Fig. 10. The resultant of forces P and C_f acts along the line O – O' that represents the direction of the possible splitting line (second branch of the critical crack).

According to the theory of elasticity [Timoshinko 1995], a splitting

failure occur if two equal and opposite forces acts along a chord of a disk. A similar distribution of stresses is produced by the four forces acting on the circular disk shown in Fig. 10 (b).

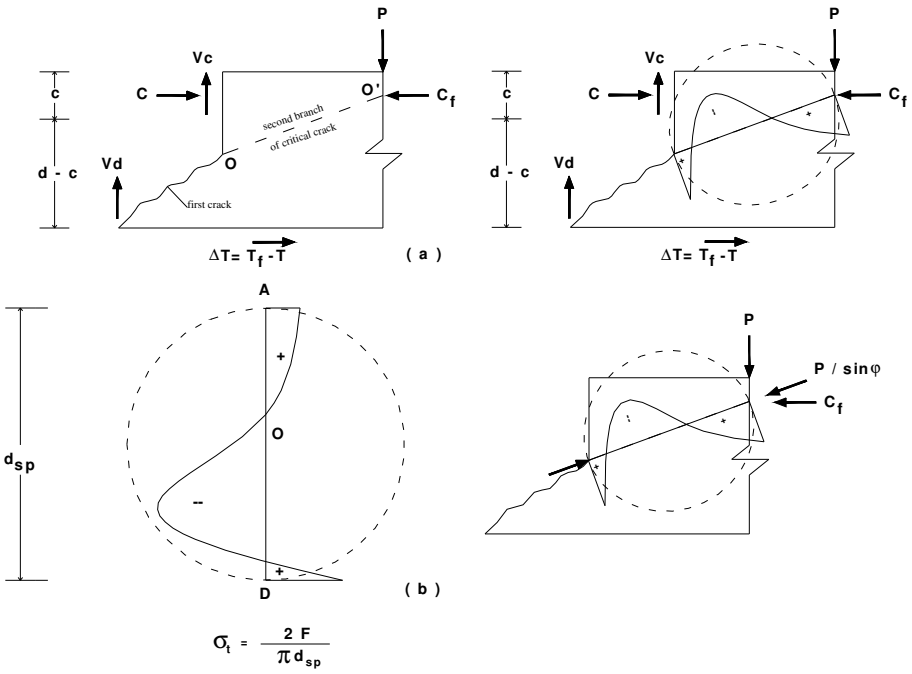

Figure 10: Splitting of concrete in circular disk.

So, the uniform normal tension stresses applied to the circumference of the disk yields the following expression (tensile splitting stress):

$$\sigma_t = \frac{2F_2}{\pi d_{sp}} \qquad (4.13)$$

Where:

σ_t : tensile splitting stress.

F : the resultant of C_f and P.

d_{sp} : diameter of the assumed disk (Cylinder).

The direct application of this theoretical model to the case of slender beams implies that the distribution of normal stresses along the line of the second branch of the critical diagonal crack has a shape similar to the one shown in Fig. 11. These stresses compose a group of forces in self-equilibrium (i.e., forces not balancing any external load). The normal stress at the beginning of the second branch is always tensile with a value given by

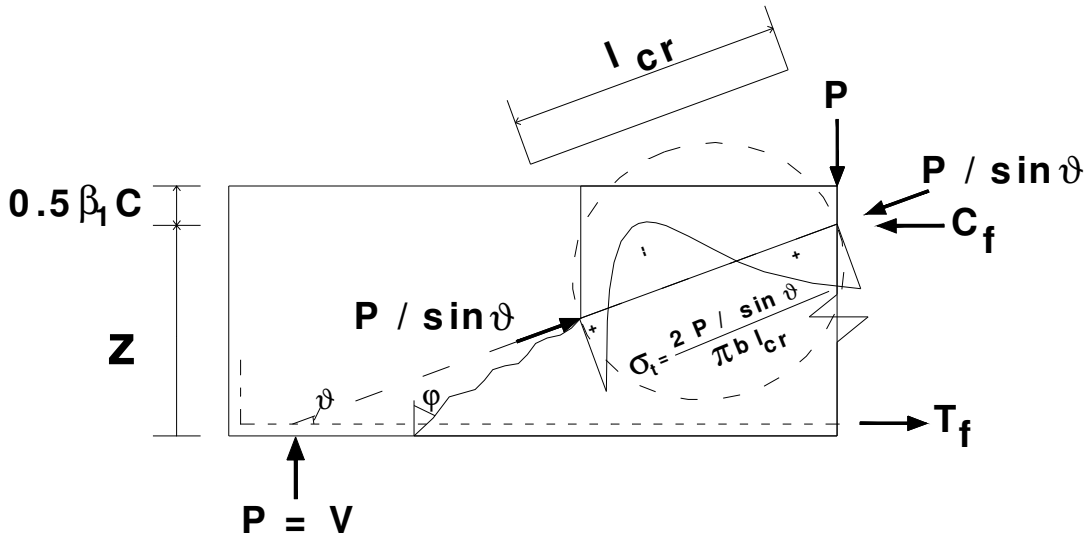

Figure 11. Distribution of normal stresses along line of second branch of critical crack.

$$\sigma_t = \frac{2P/\sin\theta}{\pi b l_{cr}} \qquad (4.14)$$

Where l_{cr} is the length of second branch of critical diagonal crack, and θ is the angle between the diagonal line of action and the horizontal direction (Figure 11).

Equation (4.14) is resulted from Eq. 4.13 by substituting the force F by $P/\sin\theta$, the diameter d_{sp} of the disk by the length l_{cr} and the unit thickness of the disk by the width b of the beam.

When the value of the normal tensile stress given by Eq. 4.14 exceeds the splitting tensile strength f_{ct}, of concrete, an initial crack forms at this area. As the length l_{cr} becomes smaller and therefore the tensile stress σ_t, larger, this crack propagates to the area of the load point, forming the second branch of the critical diagonal crack.

Taking into account that $\sin\theta = c(1 - 0.5\beta_1)/l_{cr}$ and P = total shear force V, one can obtain the shear force of the beam, which corresponds to the formation of the second branch of the critical diagonal crack, as follows:

$$V_n = \frac{1}{2}\pi b d \frac{c}{d}\left(1 - 0.5\beta_1\right) f_{ct} \qquad (4.15)$$

Substituting β_1 by 0.72, from (4.15) one can obtain a simplified nominal shear stress, which corresponds to the formation of the critical diagonal crack

$$v_n = \frac{V_n}{bd} = \frac{c}{d} f_{ct} \qquad (4.16)$$

The shear force V_n in Eq. 4.15 and the shear stress v_n in Eq. 4.16 represent the ultimate shear force and the ultimate shear stress of a slender beam, respectively. Immediately after the formation of the second branch of the critical diagonal crack, the shear force V_d of steel bars is significantly increased due to a significant increase of the angle φ, as can be directly derived from Eq. (4.4)**.** This increase in V_d in turn results in a horizontal cleavage of the concrete cover along the reinforcement, which eventually causes the loss of force V_d. As a result, the whole shear force V is transferred to the thin concrete zone above the second branch of the critical diagonal crack. This then behaves as a cantilever eventually failing due to either shear or more commonly negative bending moment forming the well-known pattern of failure.

It is worth to note that the shear strength of slender beams, as in Eq. 4.14 shows, depends mainly on the splitting tensile strength of concrete, and secondarily on the factors affecting depth of the compression zone,

given by Eq. 4.6.

2.7 Size Effect On Shear Failure

According to the previous analysis, the diagonal shear failure in slender beams is due to a splitting of concrete, which takes place in a certain region of the beam. In this section it is argued that the problem of the size effect on diagonal shear failure can be reduced to the problem of size effect on splitting tensile failure.

Tests of broad size ranges have been conducted on cylindrical disks of constant thickness by many researchers [Zararis 1995, Bazant et al. 1991, Hasegawa et al. 1985], the results confirm the existence of size effect on split-tensile failure, and show that up to a certain critical diameter, the split-cylinder strength decreases as the diameter increases.

In the splitting of concrete occurring in slender beams, the tensile part of the length l_{cr} of the second branch of the critical diagonal Crack is considered to play the role of the diameter in split-cylinder tests. The length l_{cr} and its tensile part can be accurately calculated from the relations shown in the previous section.

An approximate estimate of l_{cr} and its tensile part can be further derived using geometrical arguments, as shown in Fig 11, where l_{cr}, is equal to 0.4a and its tensile part is equal to 0.16 a. Therefore, the size effect

on the shear failure of slender beams seems to depend on the size of the shear span *a*.

Taking into account that $a = (a/d)\ d$, the size effect in beams appears to depend not only on the size of the depth *d*, as it is commonly believed, but also on the ratio *(a/d)*.

Hasegawa et al. [1985] suggested that the nominal split-cylinder strength σ_N of a disk with a diameter *D* approximately satisfies the relation $\sigma_N = (1.20 - 1.30D)\ f_{ct}$, where D in meters, and f_{ct} = nominal split-cylinder strength of a disk with a diameter of 0.15 m. This relation is valid up to a certain critical diameter, after which the split-cylinder strength does not decrease any more, but remains about constant at a minimum value. $\sigma_N = 0.65\ f_{ct}$ Substituting the diameter *D* in the above relation, with 0.16 *a* (estimated length of the tensile part of l_{cr}) yields $\sigma_N = (1.20 - 0.20a)\ f_{ct}$. Therefore, one can consider the factor *(1.20 - 0.20a)* as the one that determines the size effect on the diagonal shear failure of slender beams, with a minimum value of 0.65.

Based on this correlation, one can adjust (4.16) to take into account the size effect as follows:

$$v_n = \frac{V_n}{bd} = \left(1.2 - 0.2\frac{a}{d}d\right)\frac{c}{d} f_{ct} \qquad (4.17)$$

Where

$$1.2 - 0.2\frac{a}{d}d \geq 0.65 \qquad (4.18)$$

3. Shear Strength of SFRC vs. RC Slender Beams

The previous formulation is applicable for both, the conventional RC and the SFRC with the following exceptions:

1. The presence of steel fibers arrests the crack formation and increases the tensile strength (or the modulus of rupture) of SFRC. So the depth of the neutral axis (value of c) is shifted upward. This shift is a function of the increase in modulus of rupture Δf_r that is also a function of the fiber content, V_f and the aspect ratio l_f/d_f.

2. Since the splitting strength of steel fiber reinforced concrete is affected by the presence of steel fibers, there is a need to search for suitable value of splitting tensile strength of SFRC.

3. The modification for the size effect can be used for SFRC beams instead of that given by Eq.4.18 accounting for the fiber index, (will be discussed in the next chapter).

3.1 c/d ratio

As mentioned earlier, the presence of steel fibers contributes in increasing the tensile strength (modulus of rupture) of SFRC elements with small increase in the concrete compressive strength. The fiber contribution in the tensile strength is presented by adding a triangular stress distribution [Rjoub and Hunaiti 2002] shown in Fig. 12 to the tension zone, with maximum value equals Δf_r, given by

$$\Delta f_r = 0.7\sqrt{f_c'}\left(1+0.65V_f\frac{l_f}{d_f}\right) \qquad (4.19)$$

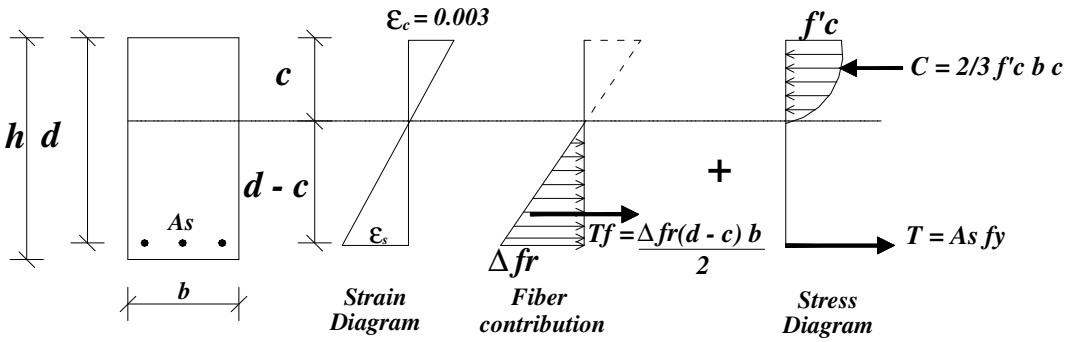

Figure 12: Stress distribution along the x-section of the SFRC beam.

The summation of forces along x-axis (Fig. 4.8) leads to the

following equation

$$C - T - T_f = 0 \tag{4.20}$$

Where:

$$C = \frac{2}{3} f_c^{'} \; b_w c$$

$$T = A_s f_y$$

$$T_f = \frac{\Delta f_r \left(d - c\right) b_w}{2}$$

Where:

T_f : Tensile force in caused by adding the steel fibers effect.

$\frac{l_f}{d_f}$: Fiber aspect ratio (length to diameter).

V_f : Fiber volume fraction %.

The substitution of the values of C, T and T_f in Eq. 4.20 yields

$$\frac{2}{3} f_c^{'} \; b_w c - \frac{\Delta f_r \left(d - c\right) b_w}{2} - A_s f_y = 0 \tag{4.21}$$

But

$$A_s f_y = A_s \varepsilon_s E_s = \rho b_w d 600 \frac{\left(d - c\right)}{c} \tag{4.22}$$

The Substitution of Eq. 4.22 into Eq. 4.21 gives

$$\frac{2}{3} f_c^{'} \, b_w c - \frac{\Delta f_r (d-c) b_w}{2} - \rho b_w d 600 \frac{(d-c)}{c} = 0 \qquad (4.23)$$

That can be written in the following form

$$\left(\frac{c}{d}\right)^2 \left(1 + \frac{0.75 \Delta f_r}{f_c^{'}}\right) + \left(900 \frac{\rho}{f_c^{'}} - \frac{0.75 \Delta f_r}{f_c^{'}}\right)\left(\frac{c}{d}\right) + 900 \frac{\rho}{f_c^{'}} = 0 \qquad (4.24)$$

If $K_1 = \frac{0.75 \Delta f_r}{f_c^{'}}$, And $K_2 = 900 \frac{\rho}{f_c^{'}}$

Then the depth of the N.A can be written as Follows

$$\left(\frac{c}{d}\right)^2 (1 + K_1) + (K_2 - K_1)\left(\frac{c}{d}\right) + K_2 = 0 \qquad (4.25)$$

3.2 Splitting Strength of SFRC

To express the splitting strength of steel fiber reinforced concrete in terms of fiber properties, the experimental splitting tensile strength, fsp of seventy-three specimens [Ashour 1992,Wahab 1991,Nima 1991,Ashour et al. 1996, Kwak et al. 2002,Marar 2002] are listed in Table 1. The specimens have fiber content ranging from 0.5% to 2% and aspect ratio (l_f /d_f) from 60 to 127.7. The concrete strength ranged from 19.68 to 101.32

MPa.

The increase in the splitting strength, Δf_{sp} caused by the addition of the fiber, for the seventy-three beams is calculated and listed in Table 1. The ratio $\Delta f_{sp}/(f_{sp})_{ACI}$ where ($f_{sp} = 0.5\sqrt{f_c'}$) is plotted against $V_f\, l_f/d_f$ and shown in Fig. 13.

The regression analysis of the plotted data lead to the following relationship that accounts for V_f and lf/d_f.

$$f_{spf} = 0.5\sqrt{f_c'}\left(1 + 0.97 V_f \frac{l_f}{d_f}\right) \qquad (4.26)$$

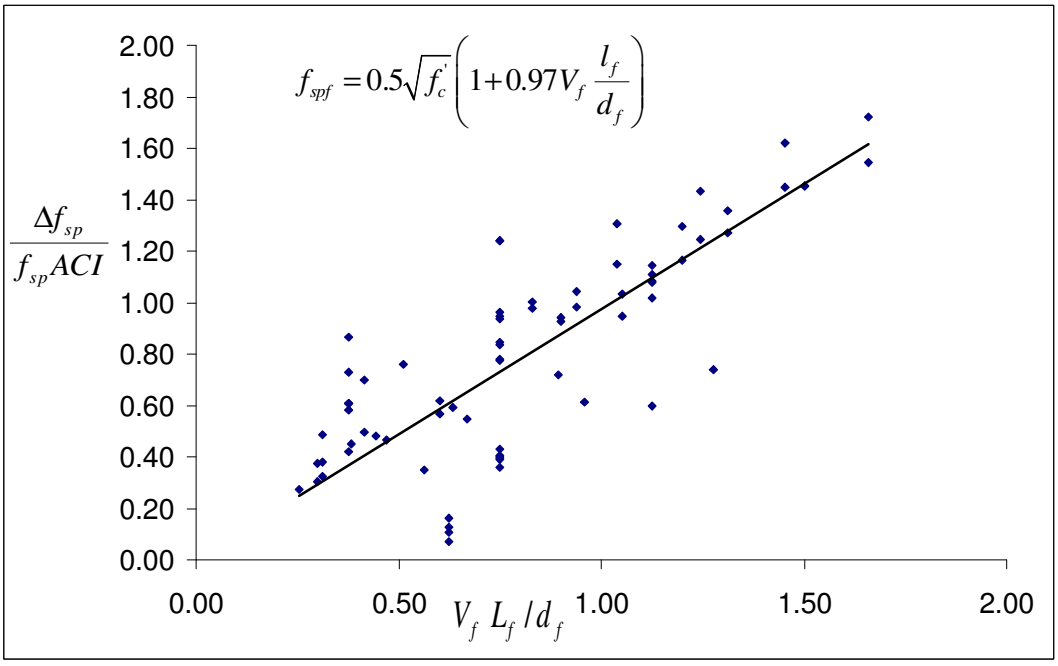

Figure 13: $\Delta f_{sp}/(f_{sp})_{ACI}$ against $V_f\, l_f/d_f$.

Table 1: Experimental data for splitting strength of SFRC.

Researcher	**Beam**	$f'c$ *(MPa)*	V_f	L_f/d_f	f_{sp} ex. (MPa)
Nima 1991	2	26.18	0.4	127.7	4.5
	3	28.565	0.7	127.7	4.6
	4	29.73	1	127.7	4.736
	5	24.614	0.4	95.75	3.6
	6	25.23	0.7	95.75	3.88
	7	25.37	1	95.75	4.06
	8	23.78	0.4	63.83	3.11
	9	24.75	0.7	63.38	3.68
	10	25.168	1	63.38	4
Wahab 1991	A2	22.63	0.5	62.5	3.15
	A3	22	1	62.5	2.6
	A4	19.68	1	62.5	2.5
	A5	20	1	62.5	2.4
	A6	28.48	1	62.5	3.1
Ashour et al. 1993	2	80.87	0.75	75	6.07
	3	82.32	1.5	75	7.24
Ashour et al. 1996	1	92	1	75	6.7
	2	92.6	1	75	6.89
	3	93.7	1	75	6.79
	4	99	0.5	75	8
	5	99.1	0.5	75	8
	6	95.4	0.5	75	9.1
	7	95.83	0.5	75	8.47
	8	95.3	1	75	10.93
	9	95.3	1	75	10.93
	10	97.53	1	75	9.7
	11	100.5	1	75	9.7
	12	96.4	1.5	75	10.2
	13	96.6	1.5	75	10.23
	14	97.1	1.5	75	9.93
	15	101.32	1	75	9.8
	16	94.5	1	75	6.8
	17	93.8	1	75	6.73
	18	95	1	75	6.63
Marar 2002	2	76.02	0.5	60	5.68
	3	78.48	1	60	6.95
	4	80.09	1.25	60	8.26
	5	84.63	1.5	60	8.93
	6	96.22	1.75	60	9.97
	7	88.97	2	60	10.83
	8	76.96	0.5	75	6.94

Table 1(cont.): Experimental data for splitting strength of SFRC

Researcher	Beam	$f'c$ (MPa)	V_f	L_f/d_f	$f_{spex.}$ (MPa)
Marar 2002	9	78.85	1	75	8.14
	10	84.48	1.25	75	9.12
	11	87.4	1.5	75	10.03
	12	89.52	1.75	75	11.16
	13	91.49	2	75	11.74
	14	78.02	0.5	83	7.51
	15	80.95	1	83	8.89
	16	86.21	1.25	83	10.71
	17	89.19	1.5	83	11.5
	18	91.73	1.75	83	12.54
	19	93.56	2	83	13.16
	20	32.66	0.5	60	3.93
	21	34.11	1	60	4.72
	22	36.28	1.25	60	5.35
	23	37.46	1.5	60	5.9
	24	39.27	1.75	60	6.1
	25	39.85	2	60	6.84
	26	33.73	0.5	75	4.12
	27	34.63	1	75	5.24
	28	36.61	1.25	75	6.18
	29	38.31	1.5	75	6.53
	30	39.63	1.75	75	7.15
	31	41.17	2	75	7.87
	32	33.99	0.5	83	4.36
	33	35.26	1	83	5.94
	34	37.09	1.25	83	6.54
	35	39.73	1.5	83	7.07
	36	41.27	1.75	83	7.86
	37	42.87	2	83	8.33
Kwak et al. 2002	FHB3	68.6	0.75	62.5	6.08
	FNB2	30.8	0.5	62.5	3.83
	FHB2	62.6	0.5	62.5	5.88

4. Shear Strength of Deep Beams

4.1 Splitting Failure Model for Deep Beams

As it is shown in the schematic presentation (Fig. 14 and Fig. 15) of the failure cracks that occur in deep beams (a/d < 2.5), the second critical crack occurs. So, the shear force is resisted by an inclined thrust between the load and the reaction, which causes splitting failure in the diagonal strut

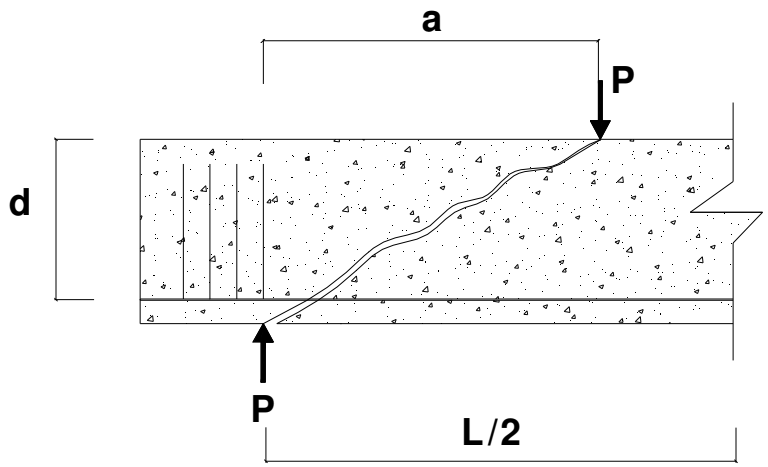

Figure 14: Typical crack pattern in deep beams.

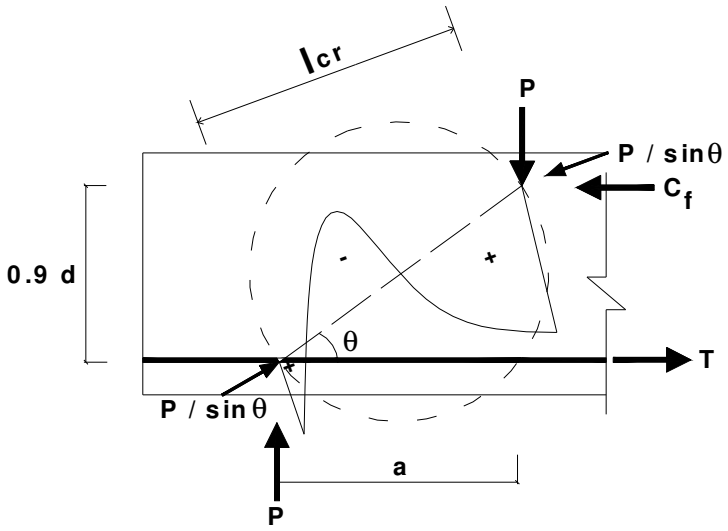

Figure 15: Distribution of normal stresses along critical crack line.

To calculate the failure shear stress in such beams due to splitting force Eq.4.14 can be applied for the case of deep beams, considering that $sin\theta = 0.9d / l_{cr}$, then the shear stress can be calculated as

$$v_n = \frac{V_n}{bd} = 1.41 f_{spf} \qquad (4.27)$$

4.2 Modified Compression Field Theory (MCFT)

Mitchell and Collins [1986] developed the Modified Compression Field Theory. The MCFT is a general model for the load-deformation behavior of two-dimensional cracked reinforced concrete subjected to shear. It models concrete considering concrete stresses in the principal directions assumed with reinforcing stresses assumed to be only axial. The concrete stress-strain behavior in compression and tension was derived originally from tests performed by [Vecchio and Collins, 1986].

The key assumption the MFCT uses to simplify is that the principal strain directions coincide with the principal stress directions. This assumption is confirmed by experimental measurements, which show that the principal directions of stress and strain are parallel within ±10.

The equilibrium conditions for the MCFT is introduced using the symmetrical cross section subjected to pure shear as shown Fig.4.12.the shear in this section is resisted by the diagonal compressive stresses, f_2 in

addition to the diagonal tensile stresses, f_1.it should be noted that the tensile stresses in the diagonally cracked concrete vary in magnitude from zero at the crack location to the peak values between the crack as shown in Fig. 16 (b).

The average value of the tensile stresses is used when formulating the equilibrium equations. From Mohr's circle shown in Fig. 16 (c), the

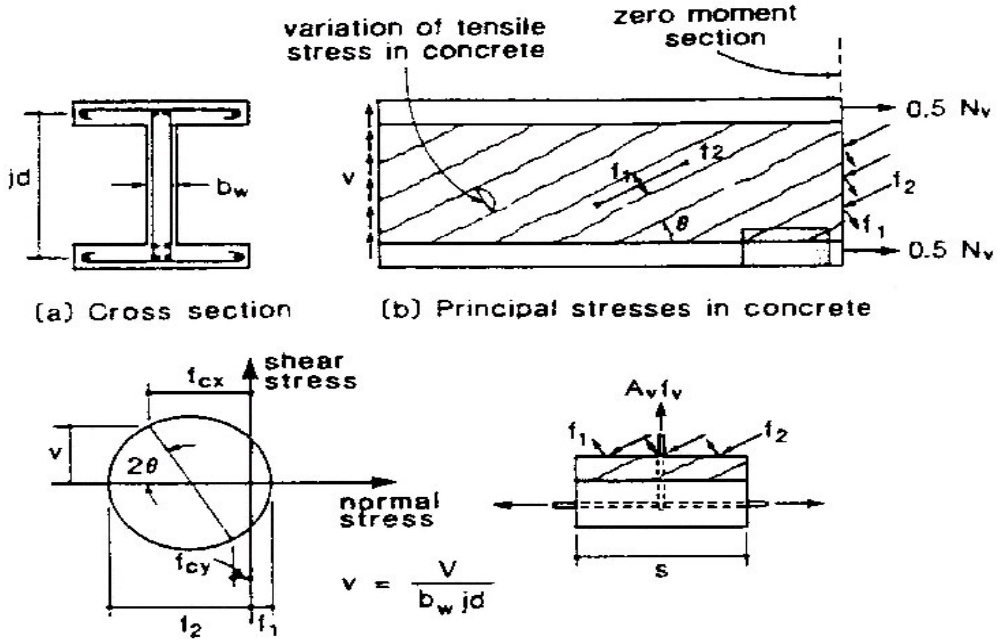

Figure 16: Eqilibrium conditions of modified compression field theory [Vecchio and Collins 1986].

following relationship for the principal compressive stress, f_2, can be derived:

$$f_2 = (\tan\theta + \cot\theta)v - f_1 \tag{4.29}$$

Where:

$$v = \frac{V}{b_w jd} \tag{4.30}$$

The diagonal compressive stresses push apart the flanges of the beam while the diagonal tensile stresses pull them together (Fig.16), the unbalanced component must be carried by tension in the web reinforcement. This equilibrium requirement can be expressed as:

$$A_v f_v = (f_2 \sin^2\theta - f_1 \cos^2\theta) \tag{4.31}$$

Where f_v is the average stress in stirrups. Substituting for f_2 from Eq.4.29 gives

$$V = f_1 b_w jd \cot\theta + \frac{A_v f_v}{s} jd \cot\theta \tag{4.32}$$

As can be seen from Eq.4.32, it is similar to ACI equation, which consists of two terms, the first is concrete contribution and the second is the reinforcement contribution.

The unbalanced longitudinal component of the diagonal concrete stresses must be equilibrated by tensile stresses in the longitudinal

reinforcement, which can be expressed as:

$$A_{sx} f_l = \left(f_2 \cos^2 \theta - f_1 \sin^2 \theta \right) b_w jd \qquad (4.33)$$

Where f_l is the average stresses in the longitudinal reinforcing bars. Substituting for f_2 from Eq.4.29 in Eq.4.33 gives

$$A_{sx} f_l = V \cot \theta - f_1 b_w jd \qquad (4.34)$$

The concrete web acts not only in compression in direction 2, but also in tension in direction 1. Therefore, the following average stress-strain relationships, based on Vecchio's experiments [Vecchio and Collins, 1982], are adopted:

$$f_2 = \frac{f_c^{'}}{0.8 + 170\,\varepsilon_1} \left(2\frac{\varepsilon_2}{\varepsilon_c^{'}} - \left(\frac{\varepsilon_2}{\varepsilon_c^{'}} \right) \right) \qquad (4.35)$$

$$f_1 = \frac{f_{cr}}{1 + \sqrt{500\varepsilon_1}} \qquad (4.36)$$

Where f_{cr} is the cracking strength of concrete. Figures 17 and 18 represent the above equations.

To deal with the local variations, the stresses that occur at a crack location will differ from the calculated average values (Fig.19), at low

shear values the ability of the crack interface to transmit the shear stress, ν_{ci}, depends on the crack width, ω.

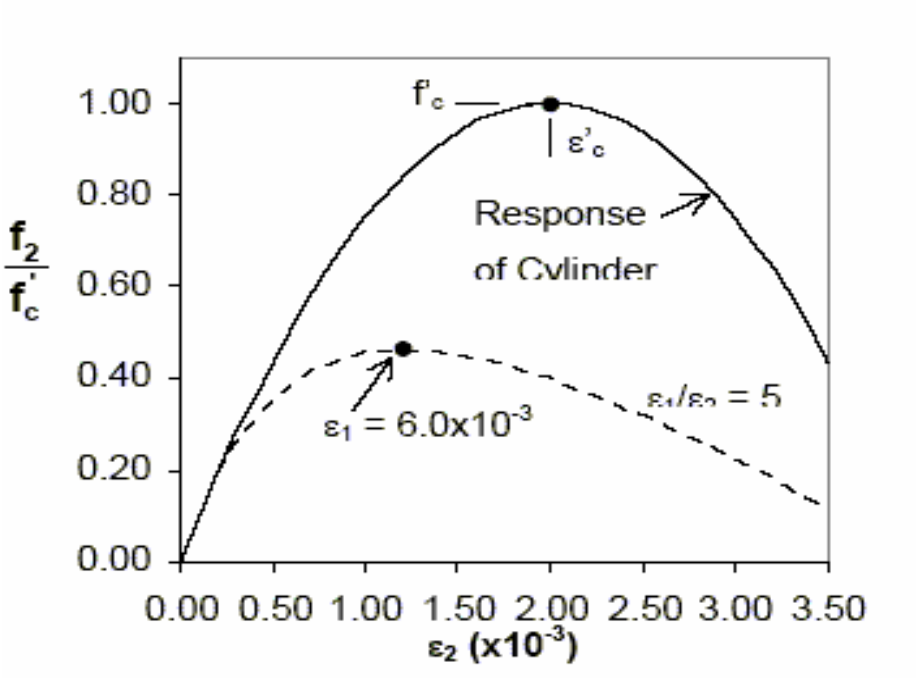

Figure 17: Compressive stress-strain relationships for cracked concrete.

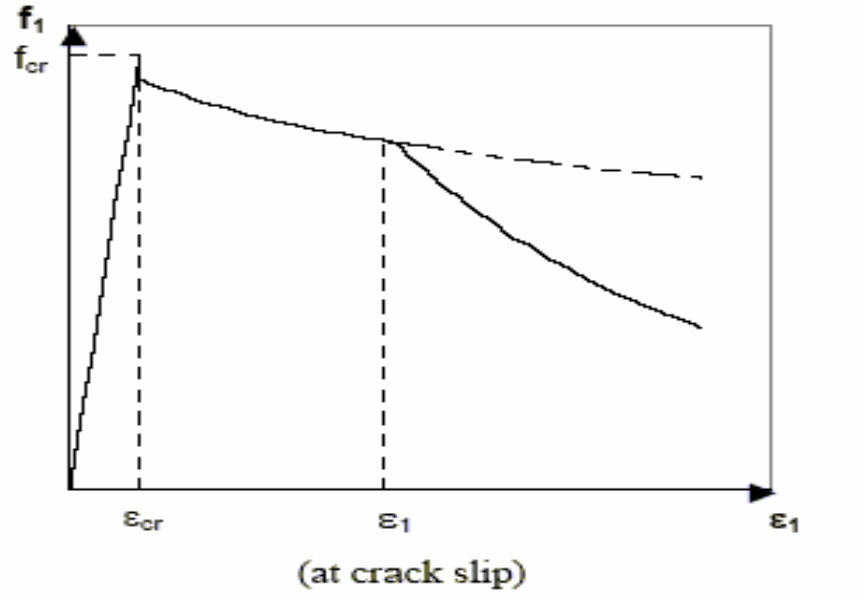

Figure 18: Average stress-strain relationship for concrete in tension.

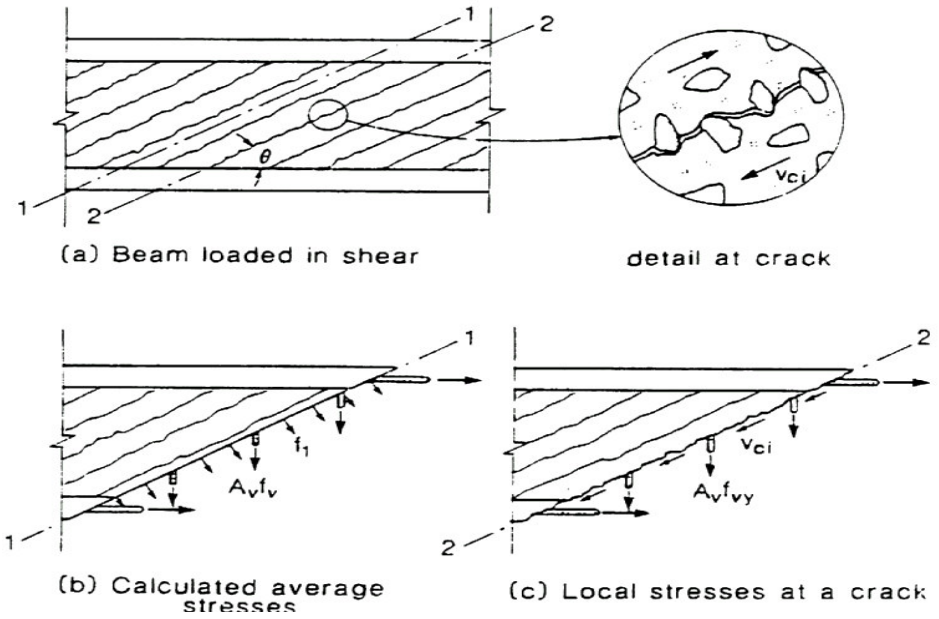

Figure 19: Transmitting forces across the crack [Vecchio and Collins 1986].

The limiting value of v_{ci} proposed by Vecchio and Collins [1986] is

$$v_{ci} \leq \frac{0.18\sqrt{f'_c}}{0.3 + \frac{24\omega}{a+16}} \qquad (4.37)$$

Where a is the maximum aggregate size in mm.

This equation, based on Walraven's [1981] experiments, was performed on various concretes whose cube strengths were 13, 37, and 59 MPa. Nevertheless, as the aggregate may fracture for high f'_c, and for low f'_c fracture goes around the aggregates.

As shown in Fig. 19 (b and c), the two sets of stresses must be statically

equivalent. The requirements that the two sets of stresses produce the same vertical force and hence to maintain this equality, f_1 must be limited to

$$f_1 = v_{ci}\tan\theta + \frac{A_v}{sb_v}\left(f_{yv} - f_v\right) \tag{4.38}$$

Eq.4.38 requires an estimation of the crack width, taken to be the crack spacing multiplied by the principal tensile strain, ε_1 as follows

$$\omega = \varepsilon_1 s_{m\theta} \tag{4.39}$$

Where:

$$s_{m\theta} = \frac{1}{\frac{\sin\theta}{s_{mx}} + \frac{\cos\theta}{s_{mv}}} \tag{4.40}$$

Finally, crack spacing, s_{mx} and s_{mv} are estimated using the formulas given by the CEBFIP Model Code (1990).

$$s_{mx} = 2\left(c_x + \frac{s_x}{10}\right) + 0.25k_1\frac{d_{bx}}{\rho_x} \tag{4.41}$$

$$s_{mv} = 2\left(c_y + \frac{s}{10}\right) + 0.25k_1\frac{d_{by}}{\rho_y} \tag{4.42}$$

Where d_b = bar diameter,

c = distance to reinforcement, Fig.20.

s = bar spacing,

$\rho_y = Ay/(bws)$,

$\rho_x = Ax/Ac$, and

k_1 = 0.40 for deformed bars or 0.8 for plain bars.

4.2.1 Shear Strength of SFRC Deep Beams Using MCFT

In order to predict shear strength of SFRC deep beams using the modified compression field theory, a modification regarding shear stress transmitted across cracks, and the type of tensile failure is done.

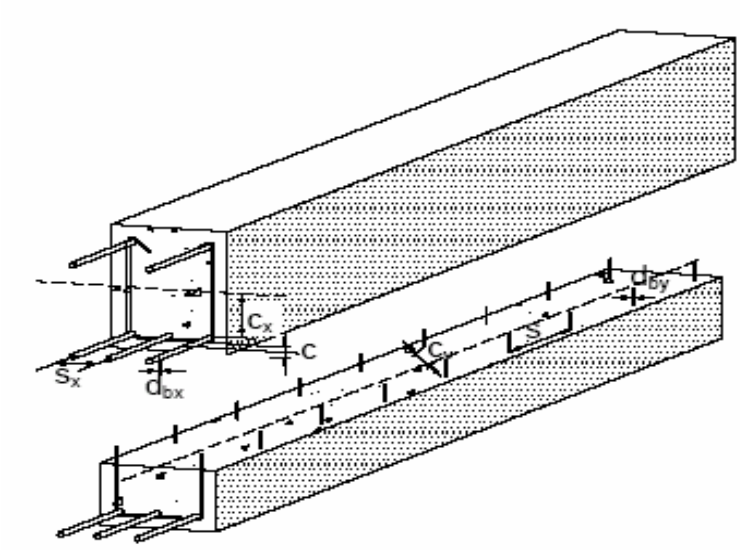

Figure 20: Parameters influencing crack spacing (Collins and Mitchell, 1997)

4.2.2 Transmitted Shear Stress across the crack

As shown in the previous sections the tensile stress, f_1 is limited to the value of v_{ci}, while with the presence of steel fiber the shear stress transmitted across the crack is increased due to the interfacial shear stress of steel fiber.

The following interfacial shear stress equation for SFRC is adopted from Narayanan and Darwish [1987].

$$v_b = 0.41\,\tau\,F \tag{4.43}$$

Where:

τ = Average fiber matrix interfacial stress taken as 4.15 MPa

F = Fiber factor = $(L_f/D_f)\,V_f\,d_f$

D_f = Fiber diameter, mm

L_f = Fiber length, mm

d_f =Bond factor equals 0.50 for round fibers, 0.75 for crimped fibers , and 1.00 for indented fibers.

Adding v_b to Eq.4.37 gives

$$v_{cif} = \frac{0.18\sqrt{f'_c}}{0.3+\frac{24\omega}{a+16}} + 0.41\tau F \tag{4.44}$$

Where: v_{cif} is the shear stress transmitted across the cracks for steel fiber reinforced concrete.

4.2.3 Tensile Strength

In the case of deep beams, the formation of cracks is affected by the splitting strength (as shown in section 4.4.1) rather than the cracking strength of concrete f_{cr}, by introducing the splitting strength of SFRC Eq.4.26 into Eq.4.36 the tensile stress f_1 becomes

$$f_1 = \frac{f_{spf}}{1+\sqrt{500\varepsilon_1}} \qquad (4.45)$$

Verification of the Proposed Model

Verification of the Proposed Model

1. General

In order to verify the capability of the proposed equation in predicting the shear strength of SFRC beams, one hundred beams are analyzed using the derived equation in chapter four. The analyzed beams were tested experimentally by several researchers. Table 2 lists the number, geometry and general properties of the tested beams. The strength of the tested beams ranged from normal to high strength concrete (from 33 to 101 MPa), with aspect ratio ranging from 62.5 to 133, and volume

Table 2: Summary of previous research.

Researcher	***No. of Beams***	***a/d***	f'_c MPa	ρ %	V_f %	***Fibre Type***
Batson et al. [1972]	36	3.2 - 5	33 - 40	3.1	0.2 – 0.9	Crimped end
Darwish et al. [1987]	25	2 - 3	39 - 80	2 – 3.7	0.25 - 3	Crimped
Ashour et al. [1992]	16	1 - 6	92 - 101	0.4 - 4.6	0.5 - 1.5	Hooked
Ghosheh [1995]	14	2 - 3.5	33 - 43	2.28	0.4 – 1.3	Hooked
Kwak et al. [2002]	9	2 - 4	30– 69	2	0.5 – 0.8	Hooked

fractions from 0.22% to 1.5%. They are reinforced by conventional steel bars of 0.37% to 3.7%, the beams are varying from deep to slender of shear span to depth ratios ranging from 1 to 6.

More details regarding the properties of the tested beams are reported in Table 3. The table shows the concrete compressive strength, the beams dimensions, and the percentage of the longitudinal steel reinforcement, the fiber properties, and the experimental shear capacity for each tested beams.

2. Analysis of slender beams

Among the beams listed in Table 2 the slender beams (where a/d >2.5) are analyzed using equation 4.16, the regression analysis is carried out to account for the size effect and the span to depth ratio, and reported in Eq. (5.1). The Fig. 21 shows the size effect on SFRC beams capacity.

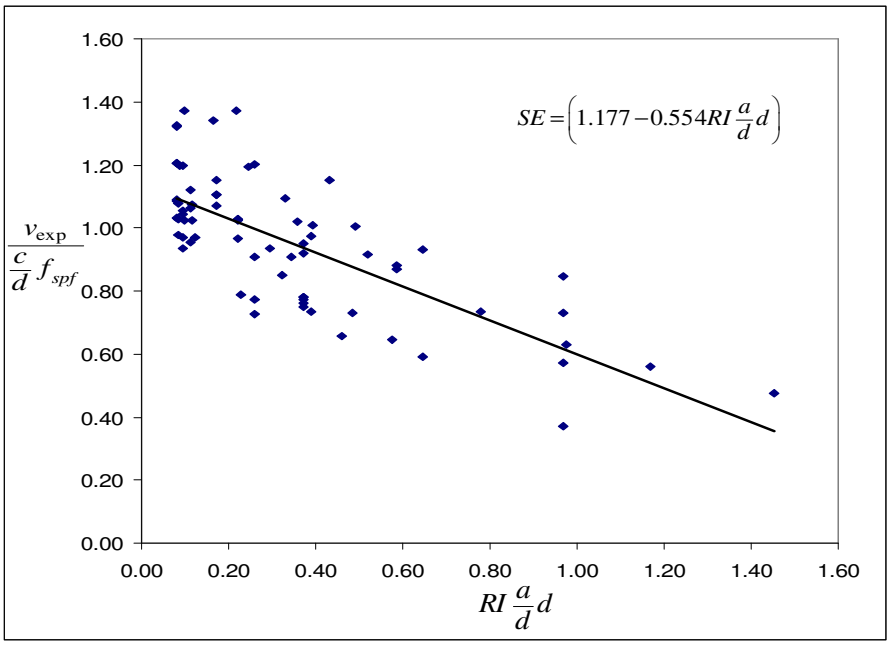

Figure 21: Size effect on SFRC beams shear strength capacity.

Table 3:Geometry and properties of the analyzed beams

Researcher	Beam	f'_c Mpa	b mm	d mm	p%	a/d	Vf%	l_f/d_f	v_{ex} MPa
Batson et al. 1972	B3	33.2	102	126	3.1	3.2	0.22	100	2.46
	C1	33.2	102	126	3.1	3.4	0.22	100	2.46
	C2	33.2	102	126	3.1	3.4	0.22	100	2.17
	C3	33.2	102	126	3.1	4	0.22	100	1.96
	D2	33.2	102	126	3.1	4	0.22	100	2.3
	D3	33.2	102	126	3.1	4	0.22	100	2.18
	E3	40.2	102	126	3.1	4	0.44	100	2.57
	F1	40.2	102	126	3.1	4	0.44	100	2.58
	F2	40.2	102	126	3.1	4	0.44	100	2.43
	F3	40.2	102	126	3.1	4	0.44	100	2.58
	G1	33.2	102	126	3.1	4.2	0.22	100	2.21
	G3	33.2	102	126	3.1	4.2	0.22	100	2.1
	L1	33.2	102	126	3.1	4.2	0.22	70	2.35
	L2	33.2	102	126	3.1	4.2	0.22	70	2.35
	L3	33.2	102	126	3.1	4.2	0.22	70	2.58
	M1	33.2	102	126	3.1	4.2	0.22	70	2.01
	M2	33.2	102	126	3.1	4.2	0.22	70	2.11
	M3	33.2	102	126	3.1	4.3	0.22	70	2
	N1	33.2	102	126	3.1	4.3	0.22	70	1.9
	N2	33.2	102	126	3.1	4.4	0.22	70	2.1
	O1	40.2	102	126	3.1	4.4	0.44	70	2.45
	P1	40.2	102	126	3.1	4.4	0.44	70	2.63
	P2	40.2	102	126	3.1	4.4	0.44	70	2.53
	P3	40.2	102	126	3.1	4.4	0.44	70	2.53
	R1	39.7	102	126	3.1	4.6	0.88	70	2.86
	R2	39.7	102	126	3.1	4.8	0.88	70	2.67
	S1	39.7	102	126	3.1	4.8	0.88	70	2.58
	X1	33.2	102	126	3.1	4.8	0.22	70	1.89
	X2	33.2	102	126	3.1	4.8	0.22	70	1.82
	X3	33.2	102	126	3.1	4.8	0.22	70	2.03
	H1	39.7	102	126	3.1	4.8	0.88	70	2.17
	H2	39.7	102	126	3.1	4.8	0.88	70	2.14
	H3	39.7	102	126	3.1	4.8	0.88	70	2.1
	11	39.7	102	126	3.1	4.8	0.88	70	2.19
	12	39.7	102	126	3.1	4.8	0.88	70	2.19
	13	39.7	102	126	3.1	5	0.88	70	2.06
Darwish et al. 1987	SF2	61.7	85	130	2	2.5	0.25	100	2.67
	SF5	39.9	85	130	2	2.5	0.25	100	2.07
	B12	61.7	85	130	2	2.5	0.5	133	3.69
	B15	67.2	85	130	2	2.5	1	133	4.42
	SF3	61.7	85	130	2	3	0.25	100	2.77
	SF6	39.2	85	130	2	3	0.25	100	1.94
	B1	61.7	85	130	2	3	0.5	133	3.23
	B30	76.7	85	130	2	3	1.5	100	3.64
	B4	79.5	85	130	2	3	2	100	3.74
	B5	77.2	85	130	2	3	2.5	100	3.76
	B6	75.8	85	130	2	3	3	100	3.85
	B7	42.3	85	130	2	3	0.5	133	1.97
	B9	41.4	85	130	2	3	1	100	2.97
	B17	55.7	85	130	3.7	3	0.5	133	2.96
	B19	42.3	85	130	3.7	3	0.5	133	2.24
	B23	71.9	85	130	3.7	3	1	133	4.37
	B27	67	85	130	3.7	3	1.5	100	4.46
	SF1	61.7	85	130	2	2	0.25	100	2.96
	SF4	39.9	85	130	2	2	0.25	100	2.41
	B11	61.7	85	130	2	2	0.5	133	4.62
	B14	67.2	85	130	2	2	1	133	5.57
	B28	59.3	85	130	2	2	0.5	100	5.46

Table 3 (cont.): Geometry and properties of the analyzed beams.

Researcher	Beam	f'_c MPa	b mm	d mm	p%	a/d	Vf%	l_f/d_f	v_{ex} MPa
Darwish et al. 1987	B29	60	85	130	2	2	1	100	6.77
	B30	67	85	130	2	2	1.5	100	7.15
	B31	55.9	85	130	2	2	2	100	6.3
Ashour et al.1992	B41L	92.6	125	215	0.37	4	1.00	75.00	0.89
	B61L	93.7	125	215	0.37	6	1.00	75.00	0.56
	B40.5A	95.4	125	215	2.84	4	0.50	75.00	2.27
	B60.5A	95.83	125	215	2.84	6	0.50	75.00	1.95
	B41A	97.53	125	215	2.84	4	1.00	75.00	3.17
	B61A	100.5	125	215	2.84	6	1.00	75.00	1.96
	B41.5A	97.1	125	215	2.84	4	1.50	75.00	3.51
	B61.5A	101.32	125	215	2.84	6	1.50	75.00	1.98
	B61M	95	125	215	4.58	6	1.00	75.00	2.93
	B10.5A	99	125	215	2.84	1	0.5	75	9.09
	B20.5A	99.1	125	215	2.84	2	0.5	75	4.82
	B11A	96.3	125	215	2.84	1	1	75	12.74
	B21A	95.3	125	215	2.84	2	1	75	6.06
	B11.5A	96.4	125	215	2.84	1	1.5	75	13.95
	B21.5A	96.6	125	215	2.84	2	1.5	75	7.21
	B21M	94.5	125	215	4.58	2	1	75	6.73
Ghosheh 1995	B6	40.11	150	175	2.28	2.5	0.375	75	1.97
	B7	42.67	150	175	2.28	2.5	0.5	75	2.95
	B8	33.5	150	175	2.28	2.5	0.75	75	2.86
	B9	40.47	150	175	2.28	2.5	1	75	3.03
	B11	40.85	150	175	2.28	3	0.75	75	2.32
	B12	33.5	150	175	2.28	3	1	75	2.70
	B13	40.47	150	175	2.28	3	1.25	75	3.09
	B15	40.11	150	175	2.28	3.5	0.5	75	1.71
	B16	38.64	150	175	2.28	3.5	0.75	75	2.23
	B17	41.42	150	175	2.28	3.5	1	75	1.83
	B18	35.91	150	175	2.28	3.5	1.25	75	1.94
	B2	39.7	150	175	2.28	2	0.5	75	3.14
	B3	38.64	150	175	2.28	2	0.7	75	3.51
	B4	41.42	150	175	2.28	2	1	75	3.84
Kwak et al. 2002	FHB2-3	63.8	125	212	2	3	0.50	62.50	3.09
	FHB3-3	68.6	125	212	2	3	0.75	62.50	3.4
	FHB2-4	63.8	125	212	2	4	0.50	62.50	2.41
	FHB3-4	68.6	125	212	2	4	0.75	62.50	2.74
	FNB2-3	30.8	125	212	2	3	0.50	62.50	2.55
	FNB2-4	30.8	125	212	2	4	0.50	62.50	2
	FHB2-2	63.8	125	212	2	2	0.5	100	5.09
	FHB3-2	68.6	125	212	2	2	0.75	100	5.44
	FNB2-2	30.8	125	212	2	2	0.5	100	4.04

$$SE = \left(1.177 - 0.554 RI \frac{a}{d} d\right) \qquad (5.1)$$

Where: $RI = V_f \frac{L_f}{d_f}$

So introducing the size effect given by Eq. (5.1) to Eq. (4.27) yields Eq. (5.2) that gives better prediction for shear strength of SFRC beams.

$$v_n = \frac{V_n}{b_w d} = \left(1.177 - 0.554 RI \frac{a}{d} d\right) \frac{c}{d} f_{spf} \qquad (5.2)$$

The analysis of 79 beams is carried out using Eq. 5.2 and the predicted shear strength are compared with the experimental values and reported in Table 4. The table shows that the average and coefficient of variation for the ratio $v_{ex} / v_{cal.}$ for all the tested beams are 1.02 and 0.17; respectively.

Also the experimental shear strength is plotted against the predicted strengths in Fig. 22.

Table 4:Slender beams: Experimental to calculated shear strength Ratio (Eq.5.2)

Researcher	Beam	a/d	RI	v_{ex} (MPa)	v_{cal} (MPa)	v_{ex}/v_{cal}
Batson et al. 1972	B3	3.20	0.02	2.46	2.25	1.09
	C1	3.40	0.02	2.46	2.24	1.10
	C2	3.40	0.02	2.17	2.24	0.97
	C3	4.00	0.02	1.96	2.22	0.88
	D2	4.00	0.02	2.30	2.22	1.03
	D3	4.00	0.04	2.18	2.22	0.98
	E3	4.00	0.04	2.57	2.57	1.00
	F1	4.00	0.04	2.58	2.57	1.00
	F2	4.00	0.04	2.43	2.57	0.95
	F3	4.00	0.02	2.58	2.57	1.00
	G1	4.20	0.02	2.21	2.22	1.00
	G3	4.20	0.01	2.10	2.22	0.95
	L1	4.20	0.01	2.35	2.14	1.10
	L2	4.20	0.01	2.35	2.14	1.10
	L3	4.20	0.01	2.58	2.14	1.21
	M1	4.20	0.01	2.01	2.14	0.94
	M2	4.20	0.01	2.11	2.14	0.99
	M3	4.30	0.01	2.00	2.13	0.94
	N1	4.30	0.01	1.90	2.13	0.89
	N2	4.40	0.03	2.10	2.13	0.99
	O1	4.40	0.03	2.45	2.40	1.02
	P1	4.40	0.03	2.63	2.40	1.10
	P2	4.40	0.03	2.53	2.40	1.05
	P3	4.40	0.05	2.53	2.40	1.05
	R1	4.60	0.05	2.86	2.67	1.07
	R2	4.80	0.05	2.67	2.65	1.01
	S1	4.80	0.01	2.58	2.65	0.98
	X1	4.80	0.01	1.89	2.12	0.89
	X2	4.80	0.01	1.82	2.12	0.86
	X3	4.80	0.05	2.03	2.12	0.96
	H1	4.80	0.05	2.17	2.65	0.82
	H2	4.80	0.05	2.14	2.65	0.81
	H3	4.80	0.05	2.10	2.65	0.79
	11	4.80	0.05	2.19	2.65	0.83
	12	4.80	0.05	2.19	2.65	0.83
	13	5.00	0.10	2.06	2.62	0.79
	MEAN					**0.97**
	STANDARD DEVIATION					**0.10**
Darwish et al. 1987	SF2	2.50	0.05	2.67	2.22	1.20
	SF5	2.50	0.10	2.07	2.08	0.99
	B12	2.50	0.02	3.69	2.76	1.33
	B15	2.50	0.01	4.42	3.49	1.26
	SF3	3.00	0.05	2.77	2.20	1.26
	SF6	3.00	0.12	1.94	2.06	0.94
	B1	3.00	0.16	3.23	2.70	1.20
	B30	3.00	0.20	3.64	3.48	1.05
	B4	3.00	0.24	3.74	3.69	1.01
	B5	3.00	0.04	3.76	3.69	1.02
	B6	3.00	0.06	3.85	3.52	1.09
	B7	3.00	0.08	1.97	2.56	0.77
	B9	3.00	0.07	2.97	2.85	1.04
	B17	3.00	0.19	2.96	3.27	0.91
	B19	3.00	0.21	2.24	3.10	0.72
	B23	3.00	0.02	4.37	4.12	1.06
	B27	3.00	0.02	4.46	4.19	1.06
	MEAN					**1.05**
	STANDARD DEVIATION					**0.17**

Table 4(cont.): Slender beams: Experimental to calculated shear strength Ratio (Eq.5.2)

Researcher	Beam	a/d	RI	v_{ex} (MPa)	v_{cal} (MPa)	v_{ex}/v_{cal}
Ashour et.al.1992	B41L	4	0.01	0.89	1.20	0.74
	B61L	6	0.01	0.56	0.93	0.60
	B40.5A	4	0.05	2.27	2.59	0.88
	B60.5A	6	0.05	1.95	2.36	0.83
	B41A	4	0.10	3.17	2.71	1.17
	B61A	6	0.10	1.96	2.12	0.92
	B41.5A	4	0.14	3.51	2.57	1.36
	B61.5A	6	0.15	1.98	1.49	1.33
	B61M	6	0.15	2.93	2.49	1.18
	MEAN					**1.00**
	STANDARD DEVIATION					**0.27**
Ghosheh 1995	B6	2.50	0.03	1.97	2.19	0.90
	B7	2.50	0.05	2.95	2.32	1.27
	B8	2.50	0.04	2.86	2.42	1.18
	B9	2.50	0.05	3.03	2.68	1.13
	B11	3.00	0.06	2.32	2.44	0.95
	B12	3.00	0.03	2.70	2.50	1.08
	B13	3.00	0.04	3.09	2.70	1.14
	B15	3.50	0.05	1.71	2.22	0.77
	B16	3.50	0.06	2.23	2.35	0.95
	B17	3.50	0.02	1.83	2.49	0.73
	B18	3.50	0.01	1.94	2.51	0.78
	MEAN					**0.99**
	STANDARD DEVIATION					**0.18**
Kwak et al. 2002	FHB2-3	3	0.31	3.09	2.21	1.40
	FHB3-3	3	0.47	3.4	2.36	1.44
	FHB2-4	4	0.31	2.41	2.13	1.13
	FHB3-4	4	0.47	2.74	2.23	1.23
	FNB2-3	3	0.31	2.55	1.97	1.29
	FNB2-4	4	0.31	2	1.90	1.05
	MEAN					**1.26**
	STANDARD DEVIATION					**0.15**
MEAN FOR ALL TESTS						**1.02**
STANDARD DEVIATION FOR ALL TESTS						**0.17**

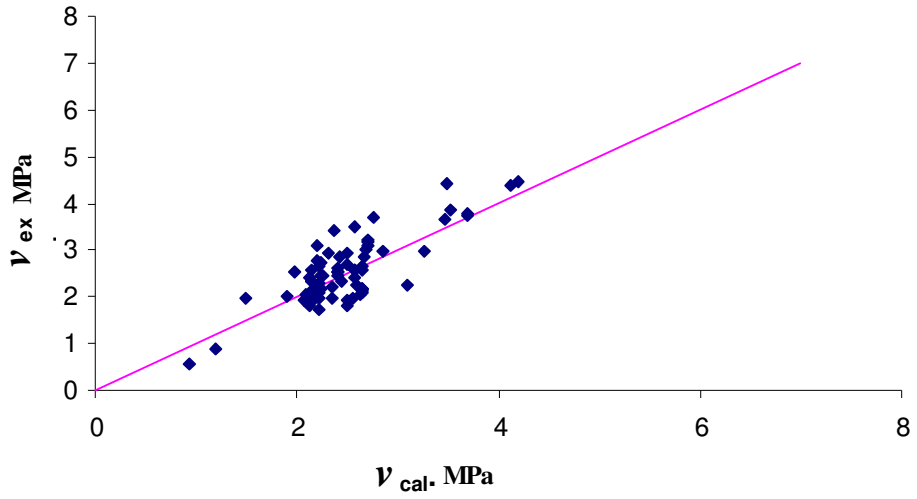

Figure 22:Experimental to predicted shear strength (Eq. 5.2)

2.1 Comparison of Shear Predictions With Other Research Works:

The shear strength using the proposed Eq. (5.2) is compared with those obtained using different equations found in the literature. And reported in Table 5.the table shows the result of analysis of beams using Sharma [1985], Mansur et al. [1986], Narayanan and Darwish [1987], Ashour et al [1992], Kwak et al. [2002].

Table 6 Shows the result of the summarizes the mean and C.O.V for v_{ex} / v_{cal} using the equations of the five research works and compares the results with those obtained from Eq. 5.2.

Table 5: Summary of the average and C.O.V of v_{ex} / v_{cal} using different equations.

Researcher	*Proposed*		*Sharma*		*Mansur et al.*		*Darwish et al.*		*Ashour et al.*		*Kwak et al.*	
	Mean	C.O.V	Mean	C.O.V	Mean	C.O.V	Mean	C.O.V	Mean	C.O.V	Mean	C.O.V
Batson e. al.	0.97	0.10	1.04	0.09	1.16	0.28	1.37	0.16	1.45	0.14	1.20	0.13
Darwish et al.	1.05	0.17	1.02	0.19	0.71	0.28	0.90	0.22	1.07	0.23	0.75	0.12
Ashour et al.	1.00	0.27	0.61	0.27	0.41	0.19	0.59	0.24	0.84	0.22	0.56	0.21
Ghosheh	0.99	0.18	0.97	0.19	0.82	0.21	0.92	0.18	1.07	0.19	0.77	0.1
Kwak et al.	1.26	0.15	0.97	0.12	1.06	0.19	1.21	0.13	1.43	0.19	1.01	0.06
All Tests	1.02	0.17	0.97	0.21	0.92	0.36	1.11	0.33	1.25	0.29	0.96	0.28

Table 6: Experimental to calculated shear strength for different researchers.

Researcher	*Beam*	*a/d*	v_{ex} *(MPa)*	v_{ex} / v_{cal}					
				Eq 5.2	Sharma 1985	Mansur et al. 1986	Narayanan and Darwish 1987	Ashour et al. 1992	Kwak et al. 2002
Batson et. al. 1972	B3	3.20	2.46	1.09	1.08	1.43	1.43	1.53	1.23
	C1	3.40	2.46	1.10	1.10	1.44	1.47	1.56	1.31
	C2	3.40	2.17	0.97	0.97	1.27	1.30	1.37	1.16
	C3	4.00	1.96	0.88	0.91	1.16	1.26	1.31	1.11
	D2	4.00	2.30	1.03	1.07	1.36	1.47	1.54	1.30
	D3	4.00	2.18	0.98	1.02	1.29	1.40	1.46	1.24
	E3	4.00	2.57	1.00	1.09	1.01	1.36	1.48	1.21
	F1	4.00	2.58	1.00	1.09	1.01	1.36	1.48	1.21
	F2	4.00	2.43	0.95	1.03	0.96	1.28	1.40	1.14
	F3	4.00	2.58	1.00	1.09	1.01	1.36	1.48	1.21
	G1	4.20	2.21	1.00	1.04	1.31	1.44	1.50	1.27
	G3	4.20	2.10	0.95	0.99	1.25	1.37	1.43	1.20
	L1	4.20	2.35	1.10	1.11	1.57	1.61	1.65	1.40
	L2	4.20	2.35	1.10	1.11	1.57	1.61	1.65	1.40
	L3	4.20	2.58	1.21	1.22	1.73	1.77	1.81	1.54
	M1	4.20	2.01	0.94	0.95	1.35	1.38	1.41	1.20
	M2	4.20	2.11	0.99	1.00	1.41	1.44	1.48	1.26
	M3	4.30	2.00	0.94	0.95	1.34	1.38	1.41	1.20
	N1	4.30	1.90	0.89	0.90	1.28	1.31	1.34	1.14
	N2	4.40	2.10	0.99	1.00	1.41	1.46	1.49	1.26
	O1	4.40	2.45	1.02	1.06	1.16	1.44	1.54	1.25
	P1	4.40	2.63	1.10	1.14	1.25	1.54	1.65	1.34
	P2	4.40	2.53	1.05	1.10	1.20	1.49	1.59	1.29
	P3	4.40	2.53	1.05	1.10	1.20	1.49	1.59	1.29
	R1	4.60	2.86	1.07	1.26	0.93	1.45	1.62	1.29
	R2	4.80	2.67	1.01	1.19	0.87	1.37	1.53	1.22
	S1	4.80	2.58	0.98	1.15	0.84	1.32	1.48	1.18
	X1	4.80	1.89	0.89	0.92	1.28	1.36	1.38	1.16
	X2	4.80	1.82	0.86	0.89	1.23	1.31	1.33	1.11
	X3	4.80	2.03	0.96	0.99	1.37	1.46	1.49	1.24
	H1	4.80	2.17	0.82	0.97	0.71	1.11	1.24	0.99
	H2	4.80	2.14	0.81	0.95	0.70	1.09	1.23	0.98
	H3	4.80	2.10	0.79	0.94	0.69	1.07	1.20	0.96
	11	4.80	2.19	0.83	0.98	0.72	1.12	1.26	1.00
	12	4.80	2.19	0.83	0.98	0.72	1.12	1.26	1.00
	13	5.00	2.06	0.79	0.93	0.67	1.07	1.20	0.95
Darwish et al. 1987	SF2	2.50	2.67	1.20	0.81	1.12	1.16	1.32	0.75
	SF5	2.50	2.07	0.99	0.78	1.07	1.05	1.15	0.71
	B12	2.50	3.69	1.33	1.12	0.92	1.19	1.42	0.86
	B15	2.50	4.42	1.26	1.29	0.64	1.00	1.23	0.81
	SF3	3.00	2.77	1.26	0.88	1.18	1.26	1.46	0.95
	SF6	3.00	1.94	0.94	0.77	1.02	1.05	1.15	0.81
	B1	3.00	3.23	1.20	1.03	0.81	1.08	1.32	0.90
	B30	3.00	3.64	1.05	1.04	0.45	0.76	0.99	0.70
	B4	3.00	3.74	1.01	1.05	0.36	0.65	0.86	0.63
	B5	3.00	3.76	1.02	1.07	0.30	0.57	0.75	0.57
	B6	3.00	3.85	1.09	1.11	0.26	0.52	0.68	0.53
	B7	3.00	1.97	0.77	0.76	0.59	0.73	0.87	0.63
	B9	3.00	2.97	1.04	1.15	0.68	0.90	1.10	0.82

Table 6(cont.): Experimental to calculated shear strength for different researchers.

Researcher	*Beam*	*a/d*	v_{ex} *(MPa)*	v_{ex} / v_{cal}					
				Eq 5.2	Sharma 1985	Mansur et al. 1986	Narayanan and Darwish 1987	Ashour et al. 1992	Kwak et al. 2002
Darwish et al. 1987	B17	3.00	2.96	0.91	0.99	0.76	0.88	1.01	0.77
	B19	3.00	2.24	0.72	0.86	0.66	0.71	0.81	0.64
	B23	3.00	4.37	1.06	1.29	0.61	0.90	1.04	0.83
	B27	3.00	4.46	1.06	1.36	0.58	0.88	1.01	0.83
Ashour et al.1992	B41L	4	0.89	0.74	0.25	0.17	0.28	0.62	0.31
	B61L	6	0.56	0.60	0.17	0.11	0.18	0.44	0.20
	B40.5A	4	2.27	0.88	0.62	0.65	0.76	0.96	0.67
	B60.5A	6	1.95	0.83	0.59	0.56	0.69	0.94	0.62
	B41A	4	3.17	1.17	0.86	0.59	0.85	1.10	0.79
	B61A	6	1.96	0.92	0.58	0.36	0.54	0.77	0.51
	B41.5A	4	3.51	1.36	0.96	0.48	0.79	1.04	0.77
	B61.5A	6	1.98	1.33	0.58	0.27	0.46	0.66	0.45
	B61M	6	2.93	1.18	0.89	0.55	0.78	1.00	0.73
Ghosheh 1995	B6	2.50	1.97	0.90	0.74	0.96	0.93	1.03	0.65
	B7	2.50	2.95	1.27	1.08	1.22	1.26	1.41	0.89
	B8	2.50	2.86	1.18	1.18	1.05	1.12	1.27	0.85
	B9	2.50	3.03	1.13	1.14	0.85	1.01	1.16	0.78
	B11	3.00	2.32	0.95	0.91	0.79	0.91	1.05	0.77
	B12	3.00	2.70	1.08	1.17	0.84	0.97	1.14	0.86
	B13	3.00	3.09	1.14	1.21	0.75	0.95	1.13	0.86
	B15	3.50	1.71	0.77	0.70	0.74	0.82	0.93	0.74
	B16	3.50	2.23	0.95	0.93	0.78	0.92	1.08	0.86
	B17	3.50	1.83	0.73	0.74	0.51	0.65	0.78	0.62
	B18	3.50	1.94	0.78	0.84	0.50	0.63	0.77	0.63
Kwak et al. 2002	FHB2-3	3	3.09	1.40	0.97	1.17	1.31	1.54	1.01
	FHB3-3	3	3.4	1.44	1.03	1.01	1.25	1.51	0.99
	FHB2-4	4	2.41	1.13	0.81	0.92	1.09	1.32	0.94
	FHB3-4	4	2.74	1.23	0.89	0.82	1.06	1.34	0.95
	FNB2-3	3	2.55	1.29	1.15	1.36	1.38	1.54	1.12
	FNB2-4	4	2	1.05	0.97	1.09	1.17	1.33	1.04

The experimental shear strength is plotted against the values obtained shear using the proposed equation and compared with those obtained by other researchers, and shown in the Figures (23, 24, 25, 26 and 27).

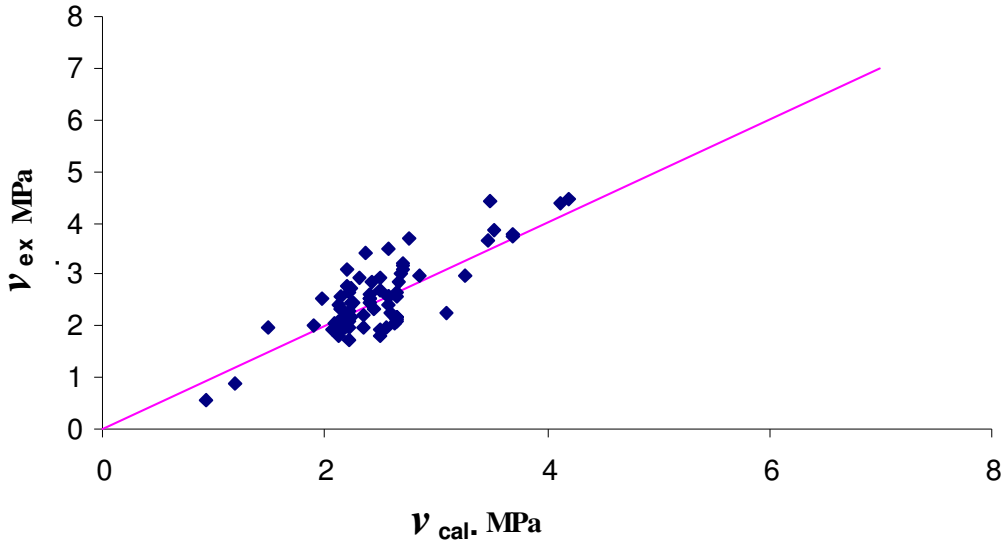

(a)

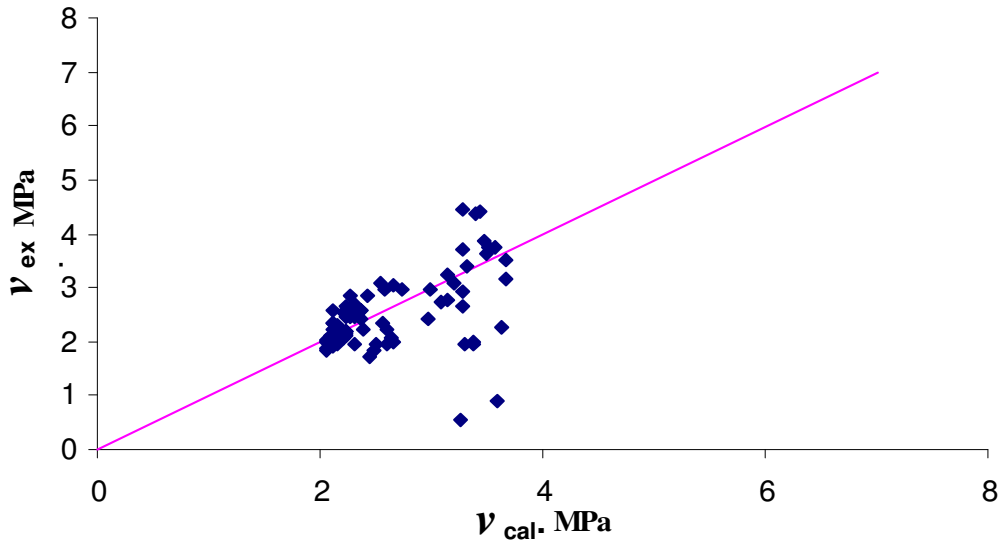

(b)

Figure 23: Shear strength: Sharma [1986] vs. the proposed equations (a) proposed equation (b) Sharma equation.

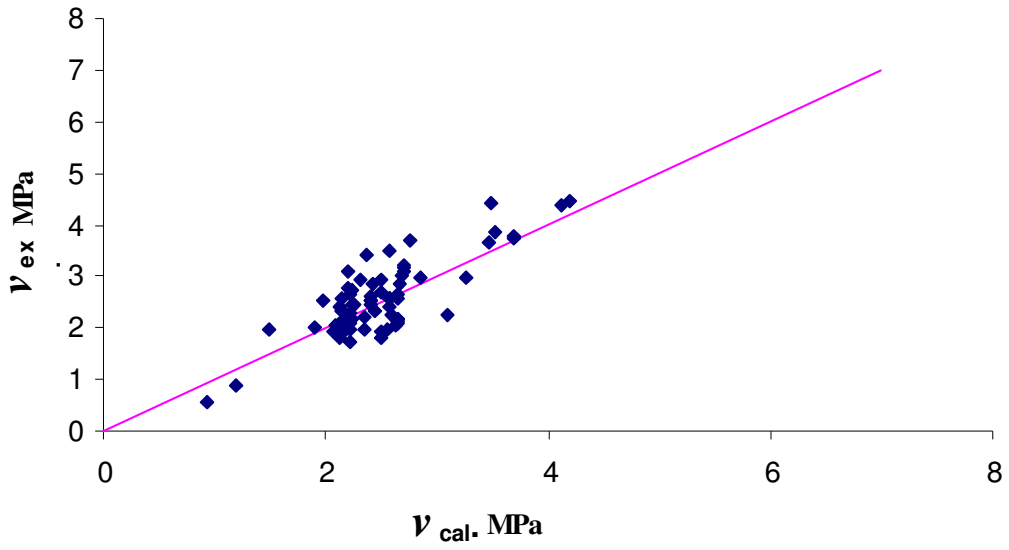

(a)

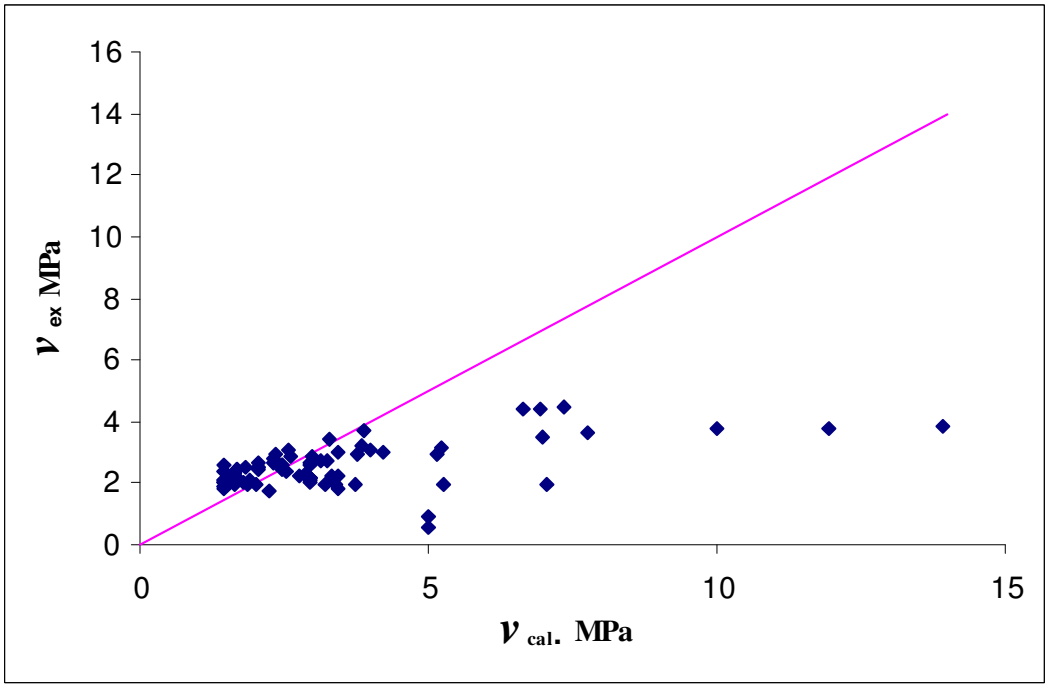

(b)

Figure 24: Shear strength: Mansur et al. [1986] vs. proposed equations (a) proposed equation (b) Mansur et al. equation.

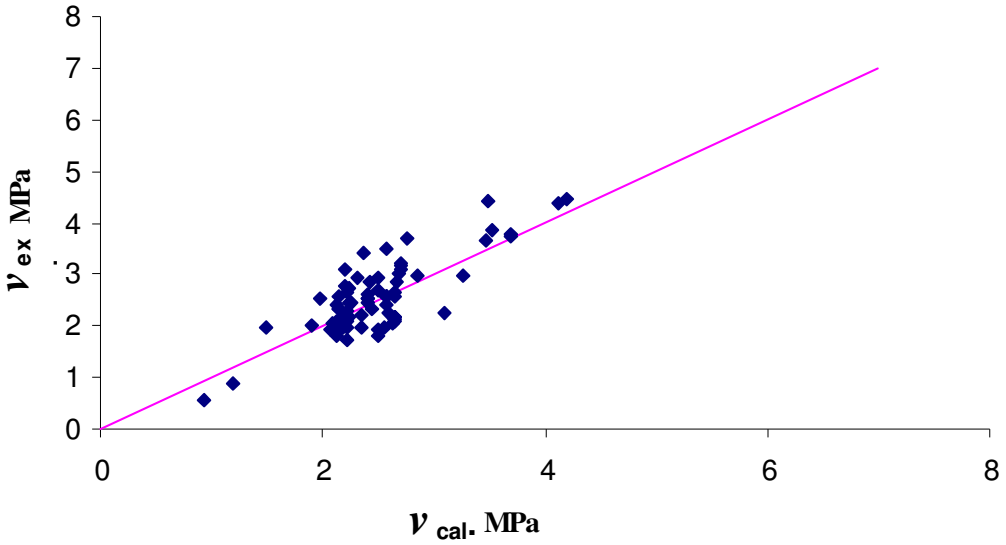

(a)

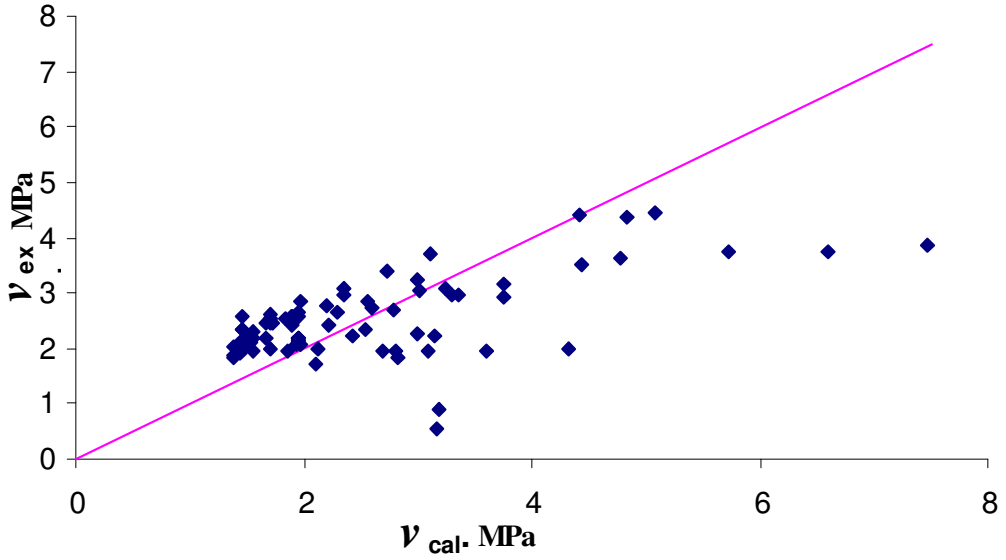

(b)

Figure 25: Shear strength: Narayanan and Darwish [1986] vs. proposed equations (a) proposed equation (b) Narayanan and Darwish equation.

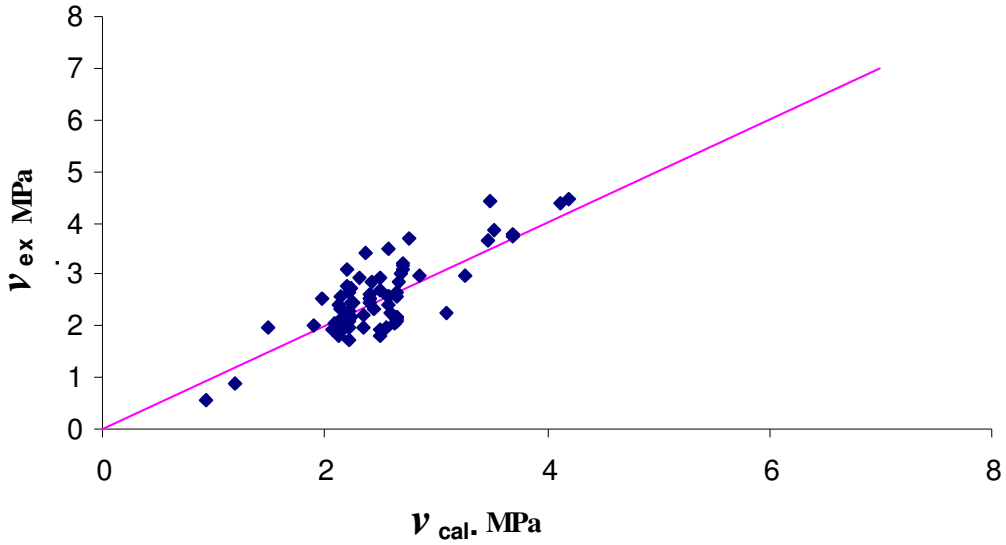

(a)

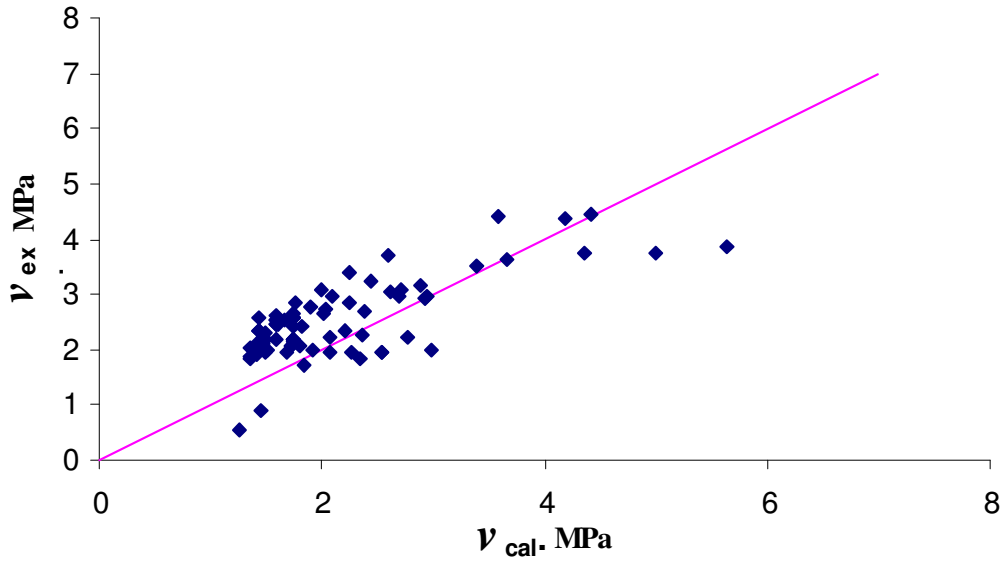

(b)

Figure 26: Shear strength: Ashour et al. [1992] vs. proposed equations (a) proposed equation (b) Ashour et al. equation.

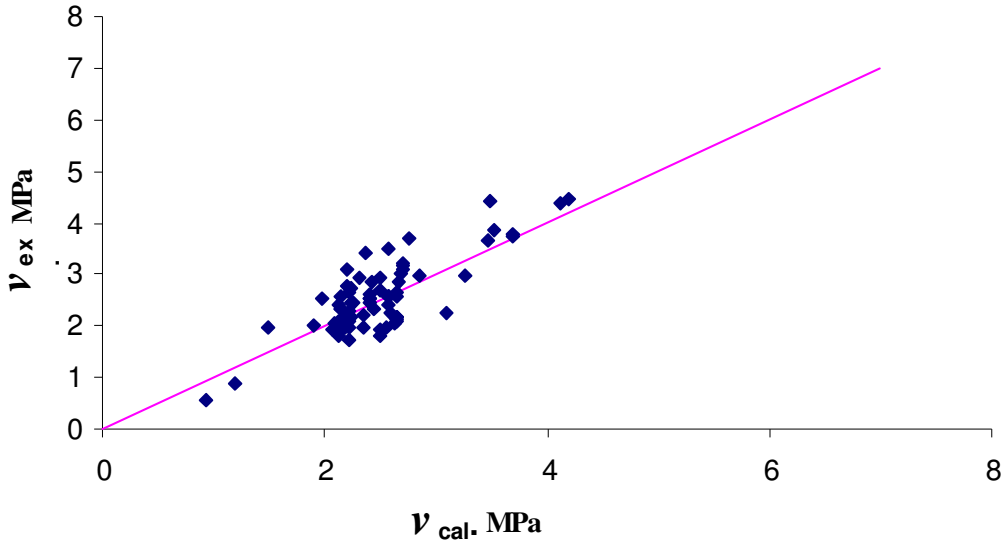

(a)

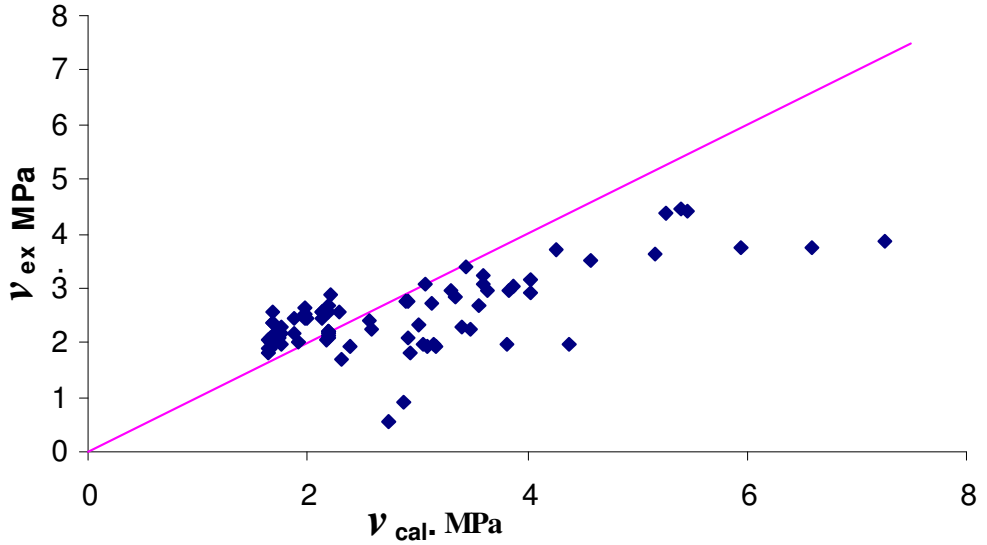

(b)

Figure 27: Shear strength: Kwak et al. [2002] and the proposed equations (a) proposed equation (b) Kwak et al. equation.

3. Analysis of Deep Beams

Twenty-one deep beams (a/d <2.5) listed in Table 5.1 and Table 5.2 are analyzed using the proposed splitting failure model (second critical crack) as follows.

3.1 Splitting Failure Model

The proposed equation for deep beams Eq.4.27 is used in the analysis of twenty-one deep beams listed in Table 2. A regression analysis is done to include the size effect factor, produced and the following equation is obtained as a modification for Eq.4.27.

$$v_f = 1.41 f_{sp} \left(A + B\, RI \left(\frac{a}{d} \right)^4 d \right) \qquad (5.3)$$

Where:

A and *B*: constants equals 0.507 and 0.0026; respectively.

The analysis of beams is carried out using Eq.5.3 and the predicted shear strengths are compared with the experimental values and reported in Table 7. The average and coefficient of variation o all the tested beams for

v_{ex} / $v_{cal.}$ are found 1.02 and 0.17; respectively. The experimental shear strength is plotted against the predicted values and shown in Fig. 28.

Table 7: Deep beam experimental to calculated shear strength using Eq.5.3

Researcher	Beam Name	a/d	RI	v_{ex} (MPa)	$v_{cal.}$(MPa)	$v_{ex}/v_{cal.}$
Darwish et al. 1987	SF1	2.00	0.25	2.96	3.51	0.84
	SF4	2.00	0.25	2.41	2.82	0.85
	B11	2.00	0.67	4.62	4.71	0.98
	B14	2.00	1.33	5.57	7.00	0.80
	B28	2.00	0.50	5.46	4.14	1.32
	B29	2.00	1.00	6.77	5.62	1.20
	B30	2.00	1.50	7.15	7.54	0.95
	B31	2.00	2.00	6.30	8.40	0.75
Ashour et al.1992	B10.5A	1.00	0.38	9.09	6.82	1.33
	B20.5A	2.00	0.38	4.82	4.95	0.97
	B11A	1.00	0.75	12.74	10.97	1.16
	B21A	2.00	0.75	6.06	6.28	0.96
	B11.5A	1.00	1.13	13.95	16.27	0.86
	B21.5A	2.00	1.13	7.21	7.83	0.92
	B21M	2.00	0.75	6.73	6.26	1.08
Ghosheh 1995	b2	2.00	0.38	3.14	3.12	1.01
	b3	2.00	0.53	3.51	3.43	1.02
	b4	2.00	0.75	3.84	4.11	0.94
Kwak et al. 2002	FHB2-2	2.00	0.50	5.09	4.35	1.17
	FHB3-2	2.00	0.75	5.44	5.33	1.02
	FNB2-2	2.00	0.50	4.04	3.03	1.34
MEAN FOR ALL TESTS						**1.02**
STANDARD DEVIATION FOR ALL TESTS						**0.17**

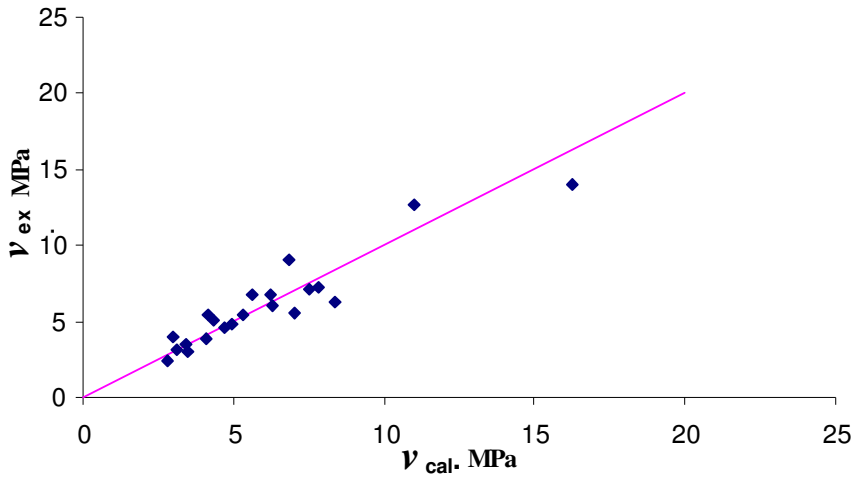

Figure 28: Deep beams experimental to calculated shear strength using equation 5.3.

3.2 Modified Compression Field Theory

The MCFT is developed to be a rational theory that predicts the stress strain responses of the cracked shear or torsion in reinforced concrete elements. In this thesis, a VISUAL BAISC program that accounts for the change in concrete properties caused by adding steel fibers is developed

The analysis of deep beams is carried out using the mentioned program to determine the shear strength. The obtained values are compared with the corresponding experimental values and reported in table 8.The listed result show that the average and coefficient of variation for the ratio $v_{ex} / v_{cal.}$ for the tested deep beams are 1.13 and 0.37; respectively. Also the experimental shear strength is plotted against the predicted value in Fig. 29.

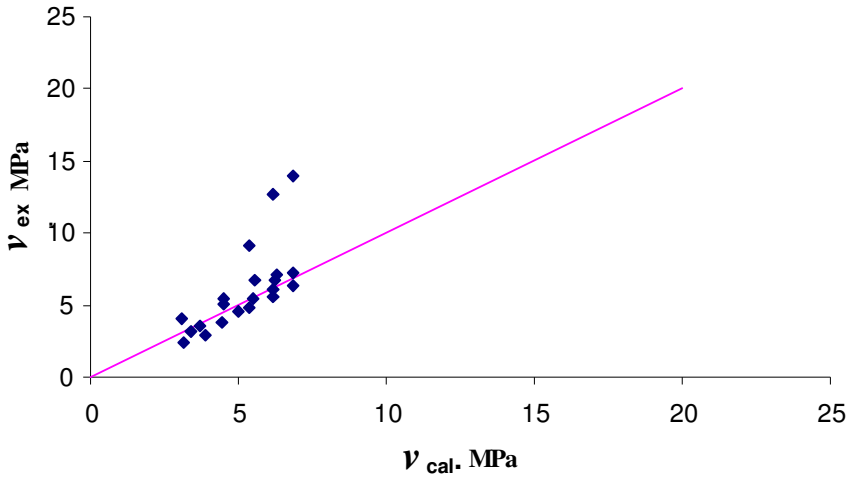

Figure 29: Experimental to calculated shear strength using MCFT.

Table 8: Deep beams: the ratio of experimental to calculated shear strength using MCFT.

Researcher	*Beam Name*	*a/d*	*RI*	v_{ex} *(MPa)*	$v_{cal.}$ *(MPa)*	v_{ex}/v_{cal}
Darwish et al. 1987	SF1	2.00	0.25	2.96	3.88	0.76
	SF4	2.00	0.25	2.41	3.12	0.77
	B11	2.00	0.67	4.62	5.02	0.92
	B14	2.00	1.33	5.57	6.19	0.90
	B28	2.00	0.50	5.46	4.53	1.20
	B29	2.00	1.00	6.77	5.53	1.22
	B30	2.00	1.50	7.15	6.31	1.13
	B31	2.00	2.00	6.30	6.83	0.92
Ashour et al.1992	B10.5A	1.00	0.38	9.09	5.39	1.69
	B20.5A	2.00	0.38	4.82	5.39	0.89
	B11A	1.00	0.75	12.74	6.20	2.05
	B21A	2.00	0.75	6.06	6.17	0.98
	B11.5A	1.00	1.13	13.95	6.84	2.04
	B21.5A	2.00	1.13	7.21	6.85	1.05
	B21M	2.00	0.75	6.73	6.21	1.08
Ghosheh 1995	b2	2.00	0.38	3.14	3.41	0.92
	b3	2.00	0.53	3.51	3.72	0.94
	b4	2.00	0.75	3.84	4.47	0.86
Kwak et al. 2002	FHB2-2	2.00	0.50	5.09	4.48	4.70
	FHB3-2	2.00	0.75	5.44	5.48	5.39
	FNB2-2	2.00	0.50	4.04	3.11	3.27
MEAN FOR ALL TESTS						***1.13***
STANDARD DEVIATION FOR ALL TESTS						***0.37***

4. Comparison of Shear Prediction With Other Work:

The shear strength using the proposed equation Eq. (5.3) compared with these obtained using several equation suggested by difference researchers and the reported in Table 9.the table shows the result of analysis of beams using Sharma [1986], Mansur et al. [1986] and Kwak et al. [2002].

Table 9: Experimental to calculated shear strength for different researchers.

Researcher	*Beam*	*a/d*	v_{ex} *(MPa)*	v_{ex} / v_{cal}				
				Eq 5.3	MCFT	Sharma 1985	Mansur et al. 1986	Kwak et al. 2002
Darwish et al. 1987	SF1	2.00	2.96	0.84	0.76	0.85	1.25	0.65
	SF4	2.00	2.41	0.85	0.77	0.86	1.25	0.65
	B11	2.00	4.62	0.98	0.92	1.33	1.18	0.87
	B14	2.00	5.57	0.80	0.90	1.53	0.84	0.84
	B28	2.00	5.46	1.32	1.20	1.60	1.69	1.10
	B29	2.00	6.77	1.20	1.22	1.97	1.33	1.16
	B30	2.00	7.15	0.95	1.13	1.97	0.98	1.04
	B31	2.00	6.30	0.75	0.92	1.90	0.74	0.87
Ashour et al.1992	B10.5A	1.00	9.09	1.33	1.69	1.73	2.36	0.63
	B20.5A	2.00	4.82	0.97	0.89	1.09	1.34	0.74
	B11A	1.00	12.74	1.16	2.05	2.47	2.29	0.84
	B21A	2.00	6.06	0.96	0.98	1.40	1.15	0.86
	B11.5A	1.00	13.95	0.86	2.04	2.70	1.91	0.87
	B21.5A	2.00	7.21	0.92	1.05	1.66	1.02	0.93
	B21M	2.00	6.73	1.08	1.08	1.56	1.24	0.87
Ghosheh 1995	B2	2.00	3.14	1.01	0.92	1.13	1.35	0.77
	B3	2.00	3.51	1.02	0.94	1.28	1.28	0.82
	B4	2.00	3.84	0.94	0.86	1.35	1.09	0.80
Kwak et al. 2002	FHB2-2	2.00	5.09	1.17	4.70	1.00	1.52	1.00
	FHB3-2	2.00	5.44	1.02	5.39	0.95	1.22	0.95
	FNB2-2	2.00	4.04	1.34	3.27	1.06	1.70	1.06

The experimental shear strength is plotted against the calculated shear using the Eq.5.3 and compared with those obtained by other researchers, and shown in Figures (30, 31 and 32,).

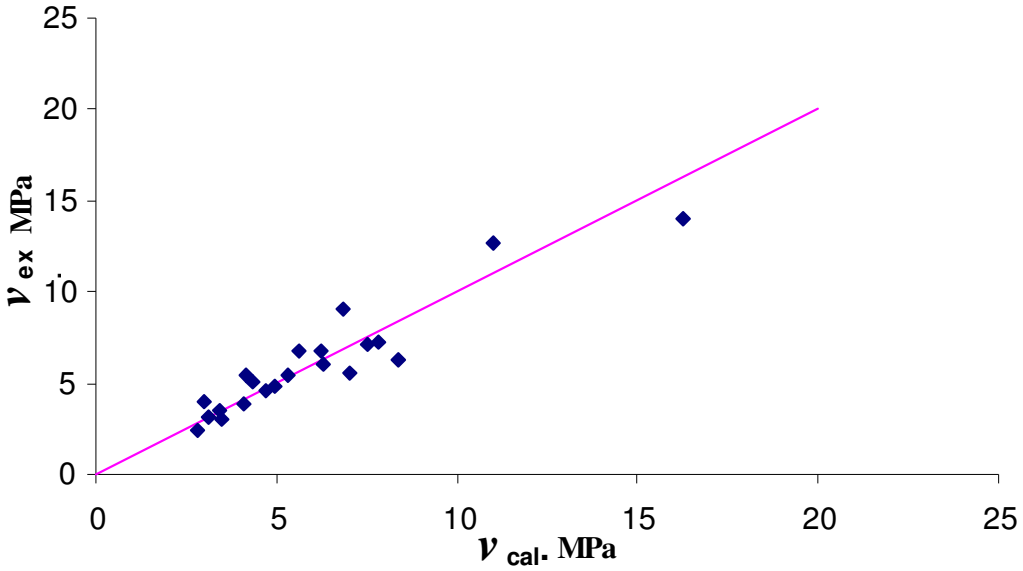

(a)

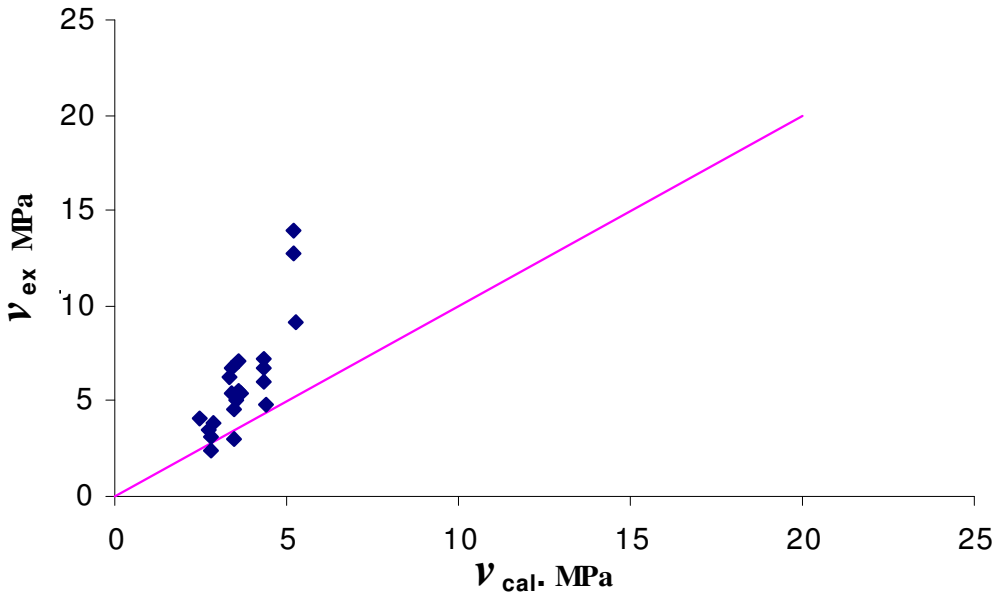

(b)

Figure 30: Comparison between Sharma [1986] and Eq.5.3 (a) Eq.5.3 (b) Sharma equation.

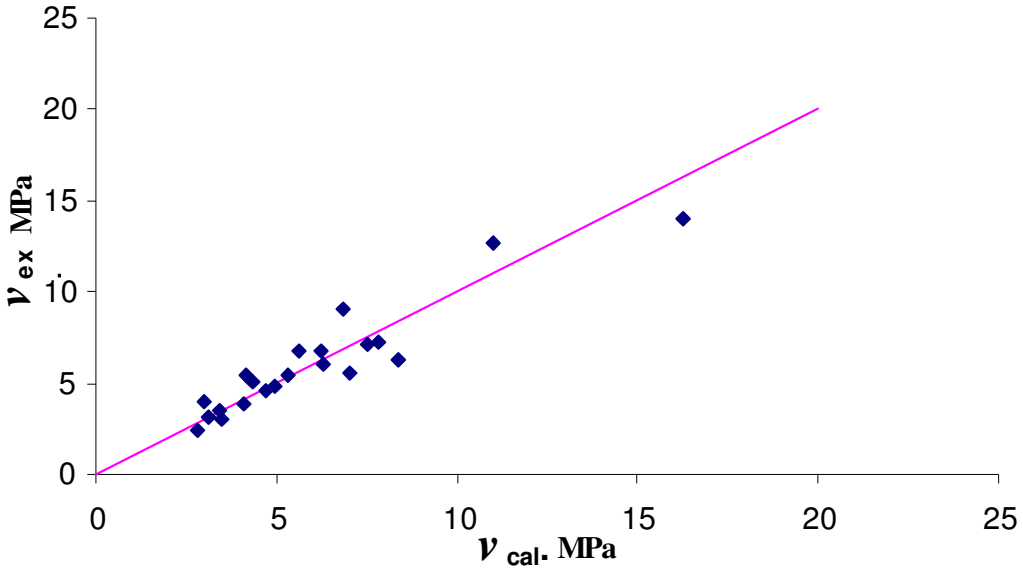

(a)

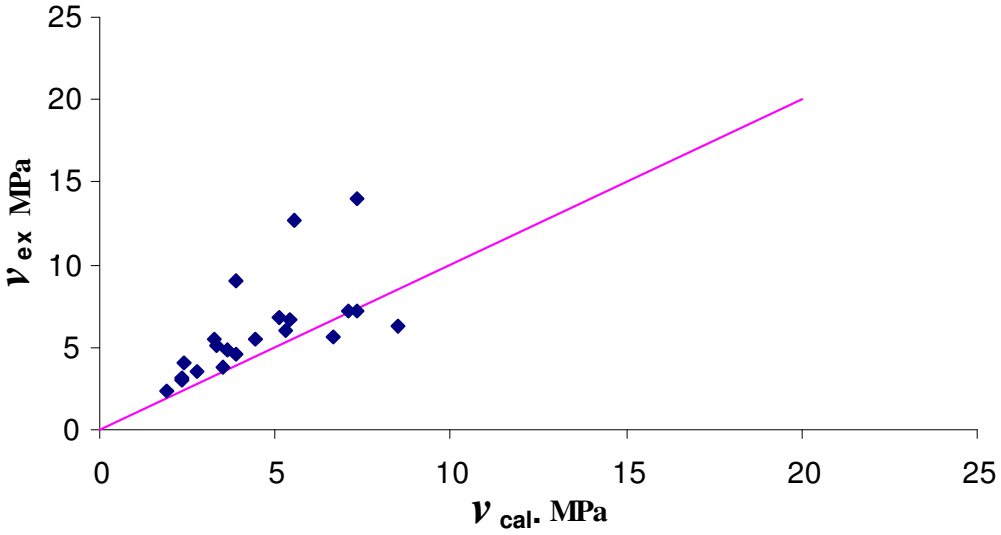

(b)

Figure 31: Comparison between Mansur et al. [1986] and Eq.5.3 (a) Eq.5.3 (b) Mansur et al. equation.

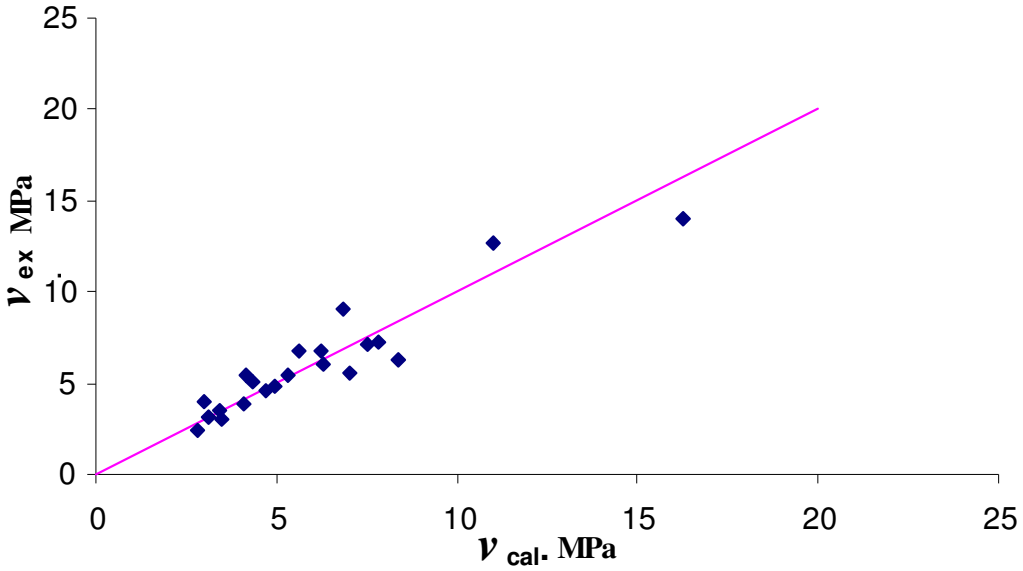

(a)

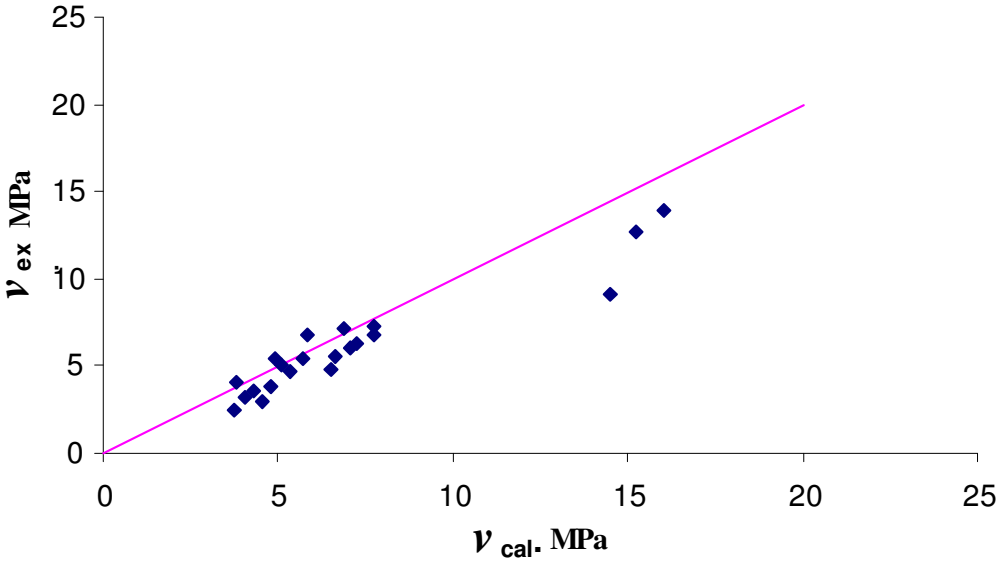

(b)

Figure 32: Comparison between Kwak et al. [2002] and Eq.5.3 (a) Eq.5.3 (b) Kwak et al. equation.

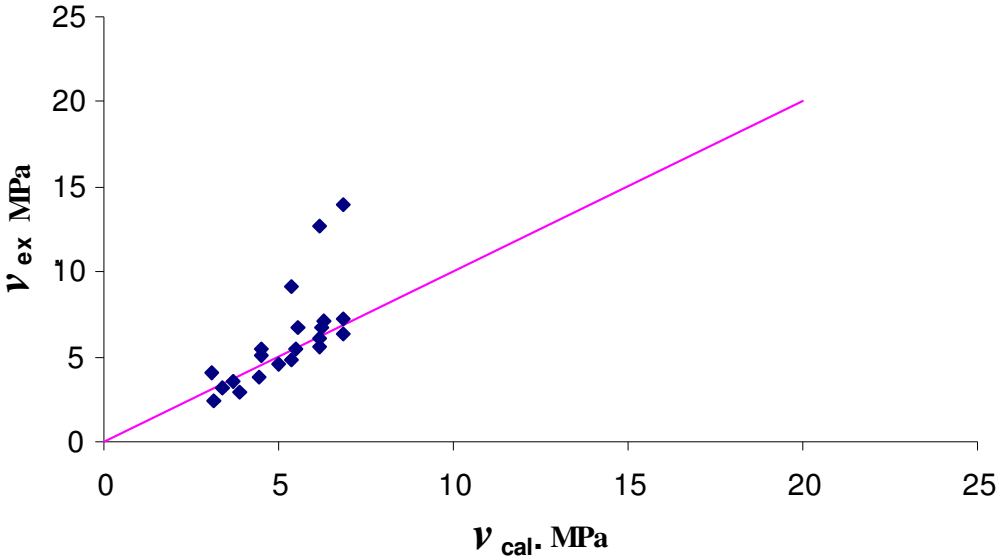

(a)

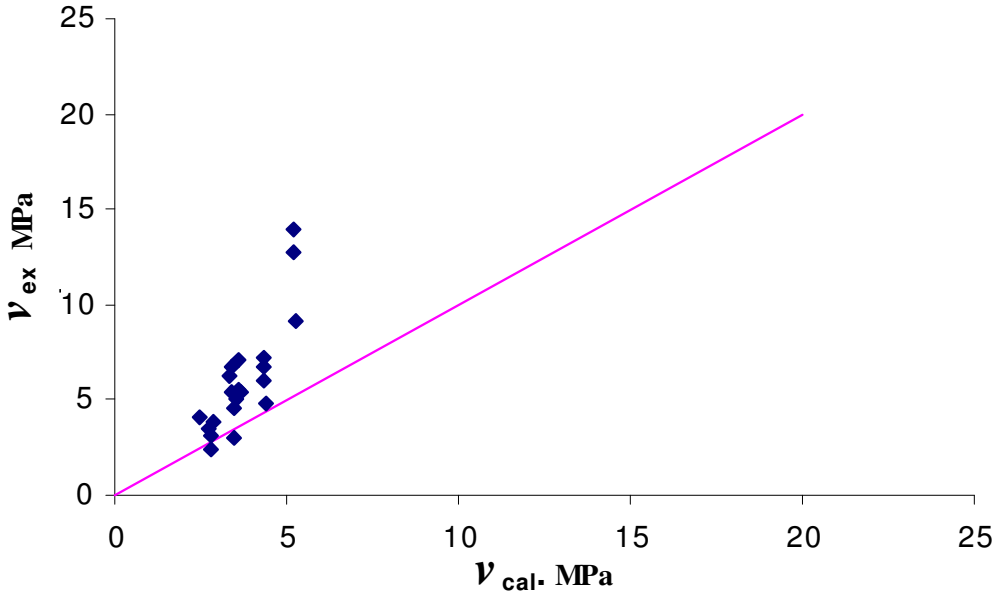

(b)

Figure 33: Comparison between Sharma [1986] and MCFT (a) MCFT (b) Sharma equation.

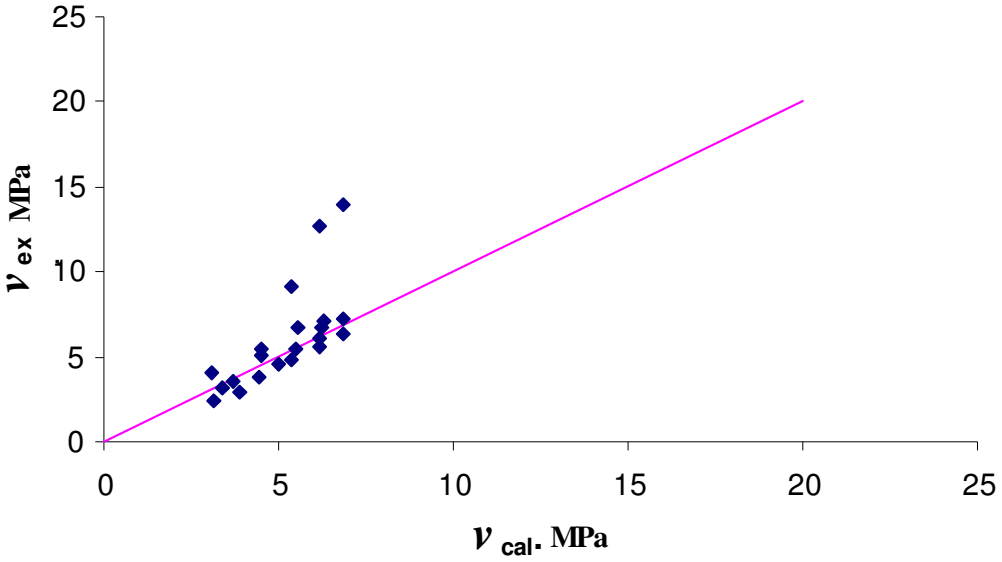

(a)

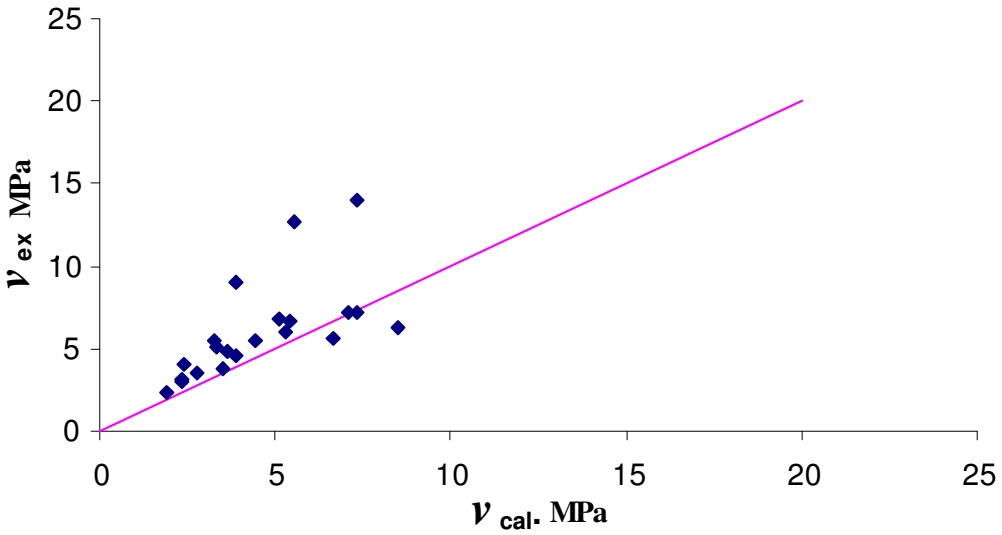

(b)

Figure 34: Comparison between Mansur et al. [1986] and MCFT (a) MCFT (b) Mansur et al. equation.

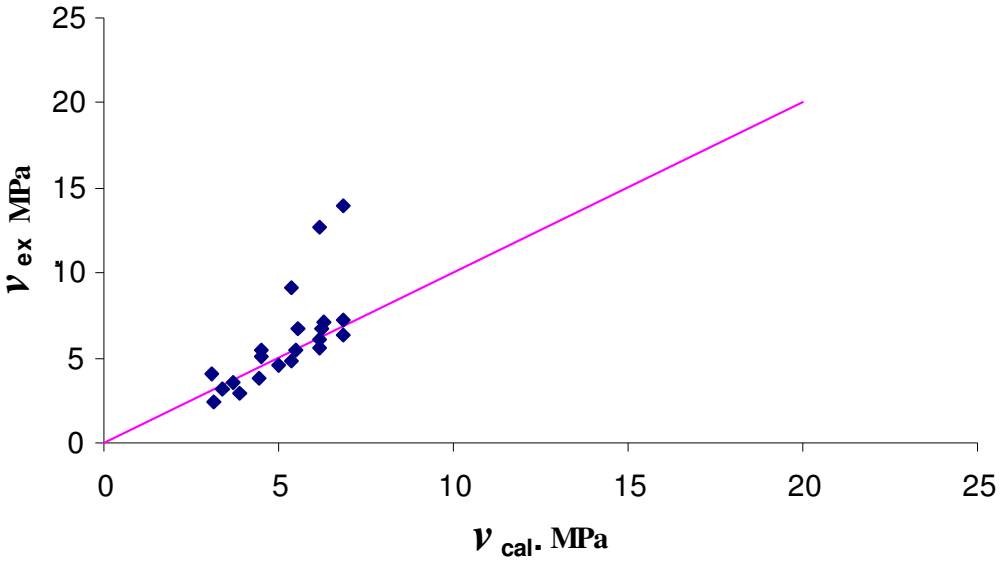

(a)

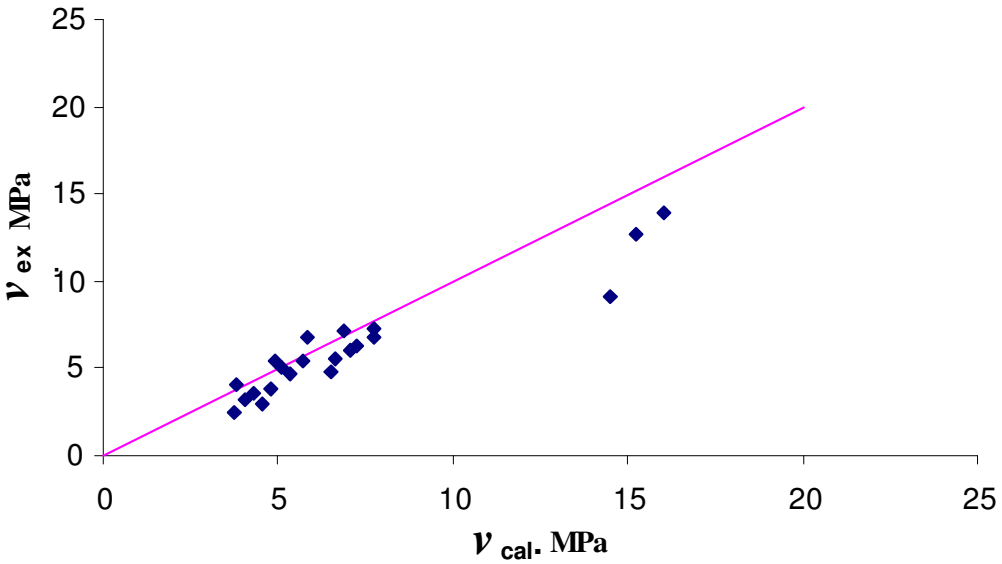

(b)

Figure 35: Comparison between Kwak et al. [2002] and MCFT (a) MCFT (b) Kwak et al. equation.

Conclusions and Recommendations for Further Works

1. Conclusions

The following conclusions are drawn from the current work:

1. A method (shear failure mechanism) has been presented, according to which the reason of shear failure of SFRC beams with out shear reinforcement, subjected to shear and bending, occurs due to splitting of concrete.
2. A new formula using the failure mechanism to predict the shear strength of SRFC slender beams is presented. The size effect is introduced to the derived formula.
3. A new formula that predicts the splitting tensile strength of SFRC cylinders is presented in this work. The formula accounts for the concrete compressive strength, the fiber content, and the fiber aspect ratio.
4. The failure mechanism approach of SFRC beams is also used to derive a formula that accounts for the ultimate shear strength of deep beams.
5. The comparison of the predicted shear strength using the new equations with the corresponding experimental values showed a good agreement.

6. The comparisons of shear predictions showed very good results compared with those found in literature.

2.Further Research Works

This new approach that is applied for rectangular SFRC beams opens new directions for further researches that can be summarized as follows:

1. A further experimental works should be conducted to study the large-scale beams especially those of high strength SFRC.
2. It is recommended to study the size effect of SFRC beams.

- ACI Committee 543., 1990." State-of-the-Art Report on Fiber Reinforced Concrete". **ACI Manual of Concrete Practice, Part 5**, American Concrete Institute, Detroit, MI, 22 pp.
- ACI Committee 544., 1994," Design Considerations for Steel Fiber Reinforced Concrete(ACI 544.4R-94)".**Manual of Concrete Practice, Part 5**, American Concrete Institute, Detroit, MI, 18 pp.
- Ashour S. A. and Wafa F. F., 1993. "Flexural Behavior of High Strength Fiber Reinforced Concrete Beams". **ACI Structural Journal**, May-Jun, Vol. 90, No. 3, pp. 279-287.
- Ashoure Sami A., Hasanain Ghazi S. and Wafa Faisal F.,1992."Shear behavior of High-Strength Fiber Reinforced Concrete beams." **ACI Structural Journal** ,VOL.89,No.2,PP 176-184.
- Balaguru. P. N., 1992."Fiber-Reinforced Rapid Setting Concrete". **Concrete International**, Feb, pp. 64-67.
- Ezeldin S. and Lowe S. R. 1991. "Mechanical Properties of Steel Fiber Reinforced Rapid-Set Materials". **ACI Materials Journal**, Jul-Aug, Vol. 88, No. 4, pp. 384-389.
- Ezeldin S. and Balaguru P. N. 1992. "Normal and High Strength Fiber-Reinforced Concrete Under Compression". **Journal of Materials in Civil Engineering**, Nov, Vol. 4, No. 4, pp. 415-429.
- Fanella D. A.and Naaman A. E. 1985. "Stress-Strain Properties of Fiber Reinforced Concrete in Compression". **ACI Materials Journal**, Jul-Aug, Vol. 82, No. 4, pp. 475-483.

- Johnston C.D. 1982. "Definition and Measurements of Flexural Toughness Parameters for Fiber Reinforced Concrete". **Cement, Concrete and Aggregates**, Winter, Vol. 4, No. 2, pp. 53-60.
- Mansur M. A., Ong C. G., and P. Paramasivam., 1986." Shear Strength of Fibrous Concrete Beams without Stirrups". **Journal of Structural Engineering**, Vol. 112, No. 9, pp. 2066-2079.
- Naaman E. 1985. "High Strength Fiber Reinforced Cement Composites". **Proceedings of MRS Symposium on Potential of Very High Strength Cement-Based Materials**, Materials Research Society; Ed. by J. F. Young; Vol. 42, pp. 217-229.
- Naaman E. 1987. "High Performance Fiber Reinforced Cement Composites". **Concrete Structures for the Future**. IABSE Symposium, Paris, pp 371-376.
- Naaman E. and Shah S. P. 1976. "Pull-Out Mechanisms in Steel Fiber-Reinforced Concrete". **Journal of Structural Engineering**, Aug, Vol. 102, No. ST8, pp. 1537-1548.
- Otter D. E. and Naaman A. E. 1988. "Fiber Reinforced Concrete Under Cyclic and Dynamic Compression Load". **Research Report, No. UMCE 88-9**, Department of Civil Engineering, University of Michigan, Ann Arbor, 178 pp.
- Shah P., Stroeven P., Dalhuisen D., and Stekelenburg P. Van. 1978., "Complete Stress-Strain Curves for Steel Fiber Reinforced concrete in Uniaxial Tension and Compression". **Testing and Test Methods of Fibre Cement Composites.** RILEM Symposium. The Construction Press, Lancaster, England, pp. 399-408.

- Shah S. P. 1991. "Do Fibers Increase the Tensile Strength of Cement-Based Matrixes", **ACI Materials Journal**, Nov-Dec, Vol. 88, No. 6, pp. 595-602.
- Shrama A.K, 1986,"Shear strength of steel fiber reinforced concrete beams",**ACI Structural Journal** ,VOL.83,No.4,PP 624-628.
- Swamy R. N., Jones R., and Chiam T. 1987. "Shear Transfer in Steel Fiber Reinforced Concrete". **Fiber Reinforced Concrete Properties and Applications**. American Concrete Institute, Detroit, MI, pp. 565-592. (ACI SP-105)
- Timoshenko, S., and Goodier, J. N.,1951. "Theory of ealsticity" ,McGrawhill, New York.
- Williamson G. R. 1974. "The Effect of Steel Fibers on the Compressive Strength of Concrete". **Fiber Reinforced Concrete**, American Concrete Institute, Detroit, MI, pp. 195-207. (ACI SP-44)
- Zararis, P. D. 1988."Faiulre mechanisms in R/C plates carrying in-plane forces.",**Journal of Structural Engineering ASCE**, VOL. 104,No. 3,pp.553-574.
- Zararis, P. D. 1995."Faiulre mechanisms in R/C plates reinforced in one way only.", **Journal of Structural Engineering ASCE**, VOL. 121, No. 8, pp.1161-1169.
- Zararis, P. D., and Papadakis G. 2001."Diagonal Shear Failure and Size Effect in RC beams with out Web Reinforcement.", **Journal of Structural Engineering ASCE**, VOL. 127, No. 7, pp.733-742.

مقاومة القص للجسور الخرسانية المسلحة المزودة بالألياف المعدنية

إعداد

محمد موسى الخواجا

إشراف

الأستاذ الدكتور ياسر الحنيطي

الدكتور محمد الرجوب

الملخص

لقد بدأ استخدام الخرسانة السلحة بالألياف المعدنية منذ عقود, حيث استخدمت الألياف لتعويض الضعف في مقاومة الشد للخرسانة غير المسلحة, فاستخدمت الألياف المنفصلة مع التسليح المستمر أحيانا وبدونه أحيانا أخرى, وقد لقيت دراسة مقاومة القص في الجيزان الخرسانية المسلحة بالألياف جهودا من الباحثين ركزت على دراسة إمكانية استبدال حديد القص (كليا أو جزئيا) بالألياف المنفصلة لما لذلك من أثر كبير على تحسين مقاومة القص للخرسانة.

وفي هذه الرسالة أجريت دراسة نظرية لمقاومة القص للخرسانة المسلحة بالألياف تم فيها استعراض النظريات السابقة لحساب مقاومة قص الجيزان, كما تم في هذه الدراسة اشتقاق معادلات لحساب مقاومة قص هذه الجيزلن بناء على آلية انهيار القصSHEAR Mechanism Failure للجيزان النحيفة (Slender Beams a/d>2.5) والتي يتضمن شكل انهيارها فرعي تشقق رئيسيين, ثم طبقت العلاقات المشتقة على الجيزان العميقة.

وحيث يتضمن انهيار الجوائز انهيارا على الفلق Splitting Failure فقد قام الباحث بدراسة تأثير وجود الألياف على مقاومة الخرسانة على الفلق Splitting Strength, واقترح لذلك علاقة تتضمن مقاومة الخرسانة و نسبة الألياف الحجمية وكذلك نسبة طولها إلى قطرها.

وقد أدخل في هذه العلاقات تأثير حجم الجوائز Size Effect of Beams, كما تم دراسة مقاومة القص باستخدام نظرية مجالات القص المعدلة بإدخال تأثير وجود الألياف على الخرسانة, وقد تم برمجة هذه النظرية مع تعديلاتها في برنامج بلغة البيسك المرئية Visual Basic . وبهدف التحقق من دقة العلاقات المقترحة تم دراسة مائة جائز(نحيف و عميق) ومقارنة المقاومة للجسور وفق العلاقات المقترحة مع تلك المقدمة من باحثين آخرين, وقد خلصت الدراسة إلى أن العلاقات المقدمة و خاصة المشتقة وفق آلية انهيار القص أعطت تقديرا لمقاومة القص مقاربا للنتائج التجريبية , ويفوق في معظم الحالات العلاقات المقدمة من باحثين آخرين لمقاومة القص في الجيزان النحيفة و العميقة.